Inorganic Chemistry

Forum Article

pubs.acs.org/IC

Lanthanide Speciation in Potential SANEX and GANEX Actinide/Lanthanide Separations Using Tetra-N-Donor Extractants

Daniel M. Whittaker,*[,†] Tamara L. Griffiths,[†] Madeleine Helliwell,[‡] Adam N. Swinburne,[†] Louise S. Natrajan,[†] Frank W. Lewis,[§] Laurence M. Harwood,[§] Stephen A. Parry,[∥] and Clint A. Sharrad*[,†,#,⊥]

[†]Centre for Radiochemistry Research, School of Chemistry, The University of Manchester, Oxford Road, Manchester M13 9PL, U.K.

[‡]School of Chemistry, The University of Manchester, Oxford Road, Manchester M13 9PL, U.K.

[§]Department of Chemistry, University of Reading, Whiteknights, Reading RG6 6AD, U.K.

[∥]Harwell Science and Innovation Campus, Diamond Light Source Ltd., Diamond House, Didcot, Oxfordshire OX11 0DE, U.K.

[#]School of Chemical Engineering and Analytical Science, The University of Manchester, Oxford Road, Manchester M13 9PL, U.K.

[⊥]Research Centre for Radwaste and Decommissioning, Dalton Nuclear Institute, The University of Manchester, Oxford Road, Manchester M13 9PL, U.K.

Supporting Information

ABSTRACT: Lanthanide(III) complexes with N-donor extractants, which exhibit the potential for the separation of minor actinides from lanthanides in the management of spent nuclear fuel, have been directly synthesized and characterized in both solution and solid states. Crystal structures of the Pr^{3+}, Eu^{3+}, Tb^{3+}, and Yb^{3+} complexes of 6,6′-bis(5,5,8,8-tetramethyl-5,6,7,8-tetrahydro-1,2,4-benzotriazin-3-yl)-1,10-phenanthroline ($CyMe_4$-BTPhen) and the Pr^{3+}, Eu^{3+}, and Tb^{3+} complexes of 2,9-bis(5,5,8,8-tetramethyl-5,6,7,8-tetrahydro-1,2,4-benzotriazin-3-yl)-2,2′-bypyridine ($CyMe_4$-BTBP) were obtained. The majority of these structures displayed coordination of two of the tetra-N-donor ligands to each Ln^{3+} ion, even when in some cases the complexations were performed with equimolar amounts of lanthanide and N-donor ligand. The structures showed that generally the lighter lanthanides had their coordination spheres completed by a bidentate nitrate ion, giving a 2+ charged complex cation, whereas the structures of the heavier lanthanides displayed tricationic complex species with a single water molecule completing their coordination environments. Electronic absorption spectroscopic titrations showed formation of the 1:2 $Ln^{3+}/L_{N_4\text{-donor}}$ species (Ln = Pr^{3+}, Eu^{3+}, Tb^{3+}) in methanol when the N-donor ligand was in excess. When the Ln^{3+} ion was in excess, evidence for formation of a 1:1 $Ln^{3+}/L_{N_4\text{-donor}}$ complex species was observed. Luminescent lifetime studies of mixtures of Eu^{3+} with excess $CyMe_4$-BTBP and $CyMe_4$-BTPhen in methanol indicated that the nitrate-coordinated species is dominant in solution. X-ray absorption spectra of Eu^{3+} and Tb^{3+} species, formed by extraction from an acidic aqueous phase into an organic solution consisting of excess N-donor extractant in pure cyclohexanone or 30% tri-*n*-butyl phosphate (TBP) in cyclohexanone, were obtained. The presence of TBP in the organic phase did not alter lanthanide speciation. Extended X-ray absorption fine structure data from these spectra were fitted using chemical models established by crystallography and solution spectroscopy and showed the dominant lanthanide species in the bulk organic phase was a 1:2 $Ln^{3+}/L_{N\text{-donor}}$ species.

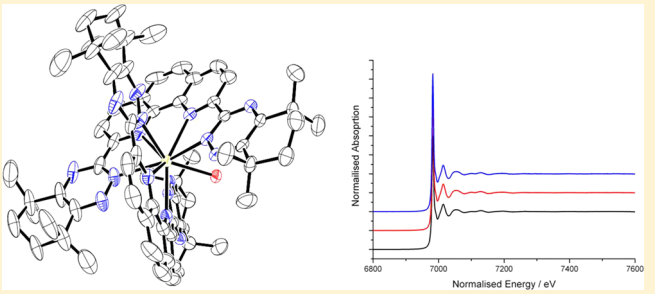

INTRODUCTION

The reprocessing of irradiated spent nuclear fuel (SNF) has been performed since the 1940s, with the initial motivation to isolate plutonium for military purposes but more recently with the purpose to separate and recover both uranium and plutonium in order to maximize the resources available to generate civil nuclear energy.[1,2] Reprocessing can also reduce the volume of nuclear waste generated with high levels of radioactivity due to the presence of long-lived radionuclides.[1,2] This separation is most commonly performed by PUREX (Plutonium URanium EXtraction, also known as Plutonium Uranium Reduction EXtraction), which is a biphasic solvent extraction process whereby $\{UO_2\}^{2+}$ and Pu^{4+}, from SNF dissolved in nitric acid (3−4 M), are extracted into an organic phase containing tri-*n*-butyl phosphate (TBP; Figure 1) in a hydrocarbon diluent (e.g., *n*-dodecane or odorless kerosene).[1−4] The uranium and plutonium are transferred into

Special Issue: Inorganic Chemistry Related to Nuclear Energy

Received: July 23, 2012

   dx.doi.org/10.1021/ic301599y | Inorg. Chem. XXXX, XXX, XXX−XXX

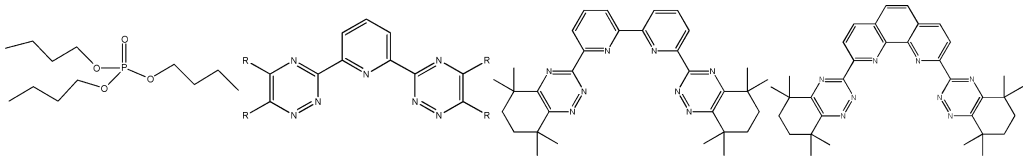

Figure 1. Structures of TBP (far left), BTP (center left), $CyMe_4$-BTBP (center right), and $CyMe_4$-BTPhen (far right).

the organic phase by forming charge-neutral complexes with TBP (i.e., $[UO_2(TBP)_2(NO_3)_2]$ and $[Pu(TBP)_2(NO_3)_4]$).[1,3−5] The plutonium, after reduction to Pu^{3+}, and uranium are then back-extracted into an aqueous phase for reuse. The aqueous phase remaining after the initial separation, known as highly active raffinate (HAR), contains over 99.9% of the fission products (e.g., lanthanide isotopes, ^{137}Cs, ^{90}Sr, ^{99}Tc) and the minor actinide activation products (neptunium, americium, and curium) with decontamination factors of 10^6−10^8 achieved by a multistage separation process.[1] The long-term management of HAR, after conversion into an appropriate wasteform, can be extremely problematic, in part due to the presence of americium and curium, which are highly radioactive and have very long half-lives (up to 10^5 years).[1,2]

Considerable efforts have been made recently to develop advanced separation methodologies in order to maximize fuel resources and reduce the impact of nuclear waste while providing a proliferation-resistant fuel cycle (i.e., no pure plutonium is isolated).[1,2,4,6−11] This forms part of the "Partitioning and Transmutation" strategy, where it is proposed that all of the actinides in SNF, including the minor actinides, can be separated and recycled as nuclear fuel. Another option is to "burn" the separated actinides, which will also result in conversion to short-lived fission product nuclides but without nuclear energy production for public consumption. This provides the added benefit of converting most of the long-lived actinides in SNF to shorter-lived fission product nuclides compared to current spent fuel management options. As a result, the "Partitioning and Transmutation" strategy can significantly reduce the time it takes for SNF to decay to radioactivity levels of natural uranium and therefore the necessary design lifetime of any nuclear waste repository.[7−11]

One of the major separation challenges that need to be overcome for this strategy to be successful is the separation of americium and curium from the lanthanide fission products. This is because the high neutron absorption cross sections of some of the lanthanide ions present in SNF both decrease the flux in a reactor and create more activation products, thereby making transmutation a less attractive option if the lanthanides cannot be separated from the actinides.[10] Achieving this separation is extremely difficult because of the chemical similarities between americium, curium, and the lanthanides, which all most commonly exist in the III+ oxidation state in solution.[12] Consequently, organic molecules that can selectively extract actinides, in particular Am^{3+} and Cm^{3+}, over the Ln^{3+} ions are of great interest, as is evident by the number of different ligand systems and processes that have been developed by various groups in the field of partitioning.[2,4,6−10,12−22] Examples include the TALSPEAK (Trivalent Actinide Lanthanide Separation by Phosphorus reagent Extraction from Aqueous Komplexes) process, which uses diethylenetriaminepentaacetic acid in a lactic acid solution to hold back Am^{3+} and Cm^{3+} in the aqueous phase while the lanthanide ions are extracted into the organic phase containing di(2-ethylhexyl)phosphoric acid,[13,14] and the TRUEX (TRans-Uranic EXtraction) process, where the addition of octyl-(phenyl)-*N*,*N*-diisobutylcarboylmethylphosphineoxide to the organic phase in the core PUREX process allows Am^{3+} and Cm^{3+} to be extracted alongside $\{UO_2\}^{2+}$ and Pu^{4+}, leaving the lanthanide ions and other fission products in the aqueous phase.[14,15]

The SANEX (Selective ActiNide EXtraction) solvent extraction process[8,9] aims to separate the minor actinides americium and curium from the lanthanide fission products remaining after plutonium and uranium removal by PUREX and fission product separation (except the lanthanides) by DIAMEX (DIAMide EXtraction)[16] using only carbon-, hydrogen-, oxygen-, and nitrogen-containing compounds as extractants, diluents, or phase modifiers. A class of molecules that showed early promise for the selective extraction of An^{3+} over Ln^{3+} in a SANEX process were the tridentate 2,6-bis(5,6-dialkyl-1,2,4-triazin-3-yl)pyridines (BTPs; Figure 1).[7,17] However, many of these extractant molecules suffered problems that precluded them from use in plant-scale extractions including poor stability, slow extraction kinetics, and inefficient back-extraction due to high An^{III} affinities.[7] Further developments in the use of triazinyl-based N-donor extractants for actinide/lanthanide separations have led to the tetradentate ligand 2,9-bis(5,5,8,8-tetramethyl-5,6,7,8-tetrahydro-1,2,4-benzotriazin-3-yl)-2,2′-bipyridine ($CyMe_4$-BTBP; Figure 1), which exhibits significant potential for use in SANEX separations, with separation factors for Am^{3+} over Eu^{3+} found to be ∼150.[7,18,19] The $CyMe_4$-BTBP extractant has been successfully tested for the extraction of genuine actinide/lanthanide feed through a 16-stage centrifugal contactor setup with excellent recoveries for americium and curium (>99.9%) but has been shown to undergo radiolytic degradation at doses that will be encountered at the high minor actinide loadings obtained in the reprocessing of, for example, fast reactor fuels.[19] The kinetics for actinide extraction with $CyMe_4$-BTBP are still relatively slow, so the addition of a phase-transfer catalyst is necessary [e.g., *N*,*N*′-dimethyl-*N*,*N*′-dioctylethylethoxymalonamide (DMDOHEMA)] if this extractant is to be used for large-scale partitioning.[19] In an attempt to improve the kinetics of extraction with these tetradentate N-donor extractants, greater conformational rigidity was enforced in the ligand backbone with the synthesis of 2,9-bis(5,5,8,8-tetramethyl-5,6,7,8-tetrahydro-1,2,4-benzotriazin-3-yl)-1,10-phenanthroline ($CyMe_4$-BTPhen; Figure 1).[20] This rigid ligand displays very high separation factors for Am^{3+} over Eu^{3+} (up to 400) with significantly faster kinetics of extraction compared to those found for $CyMe_4$-BTBP, thereby eliminating the need for a phase-transfer catalyst.[20] These high separation factors even at low acidities for the aqueous phase may prove problematic during back-extractions,[7] but the use of alternative diluents has shown that efficient back-extractions may be achievable when using the $CyMe_4$-BTPhen extractant.[20]

An alternative concept being considered in Europe for the recovery of actinides from SNF is the GANEX (Group ActiNide EXtraction) process, which is proposed to consist

dx.doi.org/10.1021/ic301599y | *Inorg. Chem.* XXXX, XXX, XXX−XXX

of two cycles.[16,21,22] Most of the uranium is removed in the first cycle, while the second cycle recovers all of the remaining actinides, mainly the transuranics neptunium through curium, concurrently in varying oxidation states (III−VI) from the fission products found in spent fuel, including the lanthanides. The GANEX process is aimed for generation IV nuclear fuel cycles, where plutonium is likely to exist in higher concentrations during partitioning processes compared to those found in the processing of SNF in current cycles.[21] The major novelty with GANEX compared to most other more technologically mature separation processes is that the plutonium is routed with the minor actinides rather than with the majority of the uranium. The separation of Am^{3+} and Cm^{3+} from the lanthanide ions in a SANEX process is already considered extremely challenging, so performing the same separation in addition to partitioning neptunium, plutonium, and any remaining uranium from all of the fission products in the second stage of the GANEX process is even more difficult. A single extractant in the organic phase is unlikely to achieve the group separation of multiple actinides in variable oxidation states with appropriate efficiencies. Consequently, the performance of multiple extractants in the organic phase, typically already established from other separation processes, has been explored for use in a GANEX process.[16,21,22] A number of different extractant combinations have been shown to have potential including *N*,*N*,*N*′,*N*′-tetraoctyldiglycolamide (TODGA; used in DIAMEX) with DMDOHEMA, TODGA with TBP, and $CyMe_4$-BTBP with TBP.[16,21,22]

The N-donor extractants $CyMe_4$-BTPhen and $CyMe_4$-BTBP have already demonstrated potential as extractants for partitioning SNF mixtures, in particular the separation of minor actinides from the lanthanides.[7,18−20] However, the mode of action of these ligands with these metal ions in extraction conditions has not been definitively established. Here, we have produced numerous Ln^{3+} complexes across the lanthanide series with both $CyMe_4$-BTPhen and $CyMe_4$-BTBP ligands using a direct synthetic approach. These complexes have been fully characterized in both solution and solid states using multiple techniques including electronic absorption spectroscopy, luminescence spectroscopy, and single-crystal X-ray diffraction (XRD). We have then used X-ray absorption spectroscopy (XAS) to probe the lanthanide (europium and terbium) species, which have been extracted into the organic phase using conditions similar to those proposed for SANEX and GANEX separation processes that use $CyMe_4$-BTPhen and $CyMe_4$-BTBP. The extended X-ray absorption fine structure (EXAFS) of the Ln L_{III}-edge XAS spectra obtained from each of these systems has been fitted to structural models established by characterization of the directly synthesized Ln^{3+} complexes with these N-donor extractants, thus providing definitive evidence for Ln^{3+} speciation in the bulk organic phase during extraction processes.

RESULTS AND DISCUSSION

Synthesis. Ln^{III} complexes of the extractant $CyMe_4$-BTPhen (see Table 1 for the list) were readily synthesized by the addition of $Ln(NO_3)_3$ (Ln = Pr, Eu, Tb, Yb) in acetonitrile to 1 mol equiv of $CyMe_4$-BTPhen in dichloromethane (DCM). The reaction solution was allowed to evaporate to dryness, leaving a powder that could be crystallized from a mixture of CH_3CN, DCM, and ethanol in a volume ratio of ∼2:2:1, where CH_3CN readily dissolves the complex, DCM acts to reduce the solubility of the complex in solution, and ethanol improves the miscibility of the solvent mixture. In all examples, yellow crystals were obtained. Elemental analysis, single-crystal XRD (see the Solid-State Structure section), and electrospray ionization mass spectrometry (ESI-MS, positive ion) indicated that, in the majority of cases, complex cations of stoichiometry 1:2 Ln^{3+}/$CyMe_4$-BTPhen with nitrate counterions were obtained even though the syntheses were conducted with equimolar amounts of $Ln(NO_3)_3$ and $CyMe_4$-BTPhen. The only exception was found during the synthesis of the Pr^{3+} complex of $CyMe_4$-BTPhen, where the major product consisted of a 1:2 Pr/$CyMe_4$-BTPhen complex cation but with a $[Pr(NO_3)_5]^{2-}$ counterion present per cationic unit. The initial crystallization of this mixture led to isolation of a small amount of this cationic species with only nitrate present as counterions, as determined by XRD (see the Solid-State Structure section). The structural determinations show that the Ln^{3+} coordination sphere is completed by a single nitrate anion for the Pr^{3+} complexes (**1** and **2**), while for the Eu^{3+}, Tb^{3+}, and Yb^{3+} complexes (**3**−**5**), a single molecule of water completes the coordination sphere (see the Solid-State Structure section). However, ESI-MS spectrometry of all the studied Ln^{3+} complexes with $CyMe_4$-BTPhen from a methanol (MeOH) solution indicates that a nitrate ion is coordinated, and there was no evidence to suggest that a water molecule was present in the coordination sphere.

Table 1. List of Synthesized Complexes

formula	compound number
$[Pr(CyMe_4\text{-BTPhen})_2(NO_3)](NO_3)_2\cdot 10H_2O$	**1**
$[Pr(CyMe_4\text{-BTPhen})_2(NO_3)][Pr(NO_3)_5]\cdot 1.63EtOH\cdot 0.75H_2O$	**2**
$[Eu(CyMe_4\text{-BTPhen})_2(H_2O)](NO_3)_3\cdot 9H_2O$	**3**
$[Tb(CyMe_4\text{-BTPhen})_2(H_2O)](NO_3)_3\cdot 9H_2O$	**4**
$[Yb(CyMe_4\text{-BTPhen})_2(H_2O)](NO_3)_3\cdot 9H_2O$	**5**
$[Pr(CyMe_4\text{-BTBP})_2(NO_3)](NO_3)_2\cdot 4EtOH\cdot H_2O$	**6**
$[Pr(CyMe_4\text{-BTBP})_2(NO_3)]_2[Pr(NO_3)_6](NO_3)\cdot 6CH_3CN$	**7**
$[Eu(CyMe_4\text{-BTBP})_2(NO_3)](NO_3)_2\cdot 4EtOH\cdot 2H_2O$	**8**
$[Eu(CyMe_4\text{-BTBP})(NO_3)_3]\cdot$toluene	**9**
$[Tb(CyMe_4\text{-BTBP})_2(H_2O)](NO_3)_3\cdot 4EtOH$	**10**

The synthesis of Ln^{3+} complexes (Ln = Pr, Eu, Tb) of $CyMe_4$-BTBP (see Table 1 for the list) was also attempted by adding a DCM solution of the ligand to 0.5 equiv of $Ln(NO_3)_3$ in MeOH. The powder obtained upon evaporation of the reaction mixture was best crystallized by slow evaporation from a 1:1:1:1 by volume mixture of toluene, isopropyl alcohol, ethanol, and DCM. The alcohols dissolve the complexes reasonably well, while the use of toluene and DCM reduces the solubility of the complexes, assists in controlling the rate of evaporation, and provides reasonable miscibility in these solvent mixtures. Characterization of the bulk crystallized material obtained from all of the attempted Ln^{3+} complexations of $CyMe_4$-BTBP indicated that a mixture of products was present, which is likely to be due to the formation of products with different combinations of Ln^{3+}/$CyMe_4$-BTBP ratios and anionic molecular ions (i.e., NO_3^-, $[Ln(NO_3)_6]^{3-}$, $[Ln(NO_3)_5]^{2-}$). However, the selection of individual crystals obtained from these reactions was able to afford the structural determination of a number of products by XRD. The vast majority of these structures indicated complex cations of 1:2 Ln^{3+}/$CyMe_4$-BTBP stoichiometry (**6**−**8** and **10**) with nitrates (**6**−**8** and **10**) and metallonitrates (**7**) present as counterions. The first structures of Ln-BTBP complexes to be isolated were

dx.doi.org/10.1021/ic301599y | Inorg. Chem. XXXX, XXX, XXX−XXX

with the ligand 6,6′-bis(5,6-diethyl-1,2,4-triazin-3-yl)-2,2′-bipyridine (C2-BTBP), and these had a single C2-BTBP molecule coordinated to the Ln^{3+} ion.[23] It was noted that in solution both 1:1 and 1:2 Ln^{3+}/C2-BTBP complexes were observed.[23] More recently, crystals of $[Eu(CyMe_4\text{-}BTBP)_2(NO_3)]^{2+}$ with a metallonitrate counterion and the charge-neutral species $[Eu(CyMe_4\text{-}BTBP)(NO_3)_3]$ were isolated by slow evaporation from a mixture of DCM and CH_3CN.[24] Our attempts to form the Eu^{3+} complex of $CyMe_4$-BTBP produced a 1:1 Eu^{3+}/$CyMe_4$-BTBP molecular species with a toluene molecule present as a solvent of crystallization (**9**) in addition to the 1:2 Eu^{3+}/$CyMe_4$-BTBP complex cation containing species but with only nitrate counterions present in the lattice. The Pr^{3+} and Eu^{3+} complexes isolated in the solid state (**6**–**9**) have one or more nitrate ions completing the coordination sphere, while only the Tb^{3+} complex of $CyMe_4$-BTBP has a water molecule in its coordination environment. The ESI-MS spectra of all of the $CyMe_4$-BTBP complexes obtained from MeOH indicated that the only intact molecular species present was $[Ln(CyMe_4\text{-}BTBP)_2(NO_3)]^{2+}$. The ESI-MS spectra of the $CyMe_4$-BTPhen complexes provide comparable results and are in agreement with similar ESI-MS studies previously performed on extracted solutions of Eu^{3+} with BTBP extractants.[25] This suggests that the 1:2:1 Ln^{3+}/$CyMe_4$-BTBP/NO_3^- complex is dominant in solution, while other compositions were only present in solution in minor quantities, if at all.

Solution Spectroscopy. The UV–visible absorption spectra of complexes **2**–**4**, isolated in a pure bulk form, dissolved in MeOH are dominated by charge-transfer transitions in the UV region of the spectra (see the Supporting Information). These transitions are most likely due to π–π^* transitions from the aromatic nature of the $CyMe_4$-BTPhen ligand. A clear difference in the spectral profile is observed between the free $CyMe_4$-BTPhen ligand and Ln^{3+} complexes, indicating that the electronic structure of the $CyMe_4$-BTPhen molecule is perturbed upon Ln^{III} coordination. Essentially no difference is observed between the spectroscopic profiles for **2**–**4**, indicating that there is little or no influence by the type of coordinating lanthanide ion on the electronic structure of the $CyMe_4$-BTPhen ligand. The limited solubility of these complexes in most common solvents precluded the study of the typically weakly absorbing f–f transitions of the lanthanides in 1-cm-path-length cells.

Titrations of $CyMe_4$-BTPhen and $CyMe_4$-BTBP with the lanthanide ions, Pr^{3+}, Eu^{3+}, and Tb^{3+} in MeOH were performed to study the lanthanide speciation behavior of these extractant molecules, in particular the equilibrium between 1:1 and 1:2 $Ln^{3+}/L_{N_4\text{-donor}}$ species. The titrations of $CyMe_4$-BTPhen with each of the lanthanides studied show that there is essentially no difference in the titration profiles with different lanthanide ions (see Figure 2 for Pr^{3+} and Supporting Information). Sharp decreases in the intensity of the absorption maxima for free $CyMe_4$-BTPhen at 261 and 295 nm with the addition of up to 0.5 equiv of $Ln(NO_3)_3$ are observed. The absorption maximum at 261 nm also shifts to ~266 nm with the addition of $Ln(NO_3)_3$. Isosbestic points are observed at 229 and 279 nm. Further additions of $Ln(NO_3)_3$, up to 3 equiv, result in a subtle decrease in the absorption intensity for most of the spectrum but with no changes in the shape of the spectral profile. This indicates that the 1:2 Ln^{3+}/$CyMe_4$-BTPhen complex forms with the initial addition of $Ln(NO_3)_3$, as expected.[23,26] The subtle changes in the spectra when more than 0.5 equiv of $Ln(NO_3)_3$ is present in solution are most likely explained by an equilibrium being established between 1:1 and 1:2 Ln^{3+}/$CyMe_4$-BTPhen species, where more 1:1 complex is likely to form with increasing additions of $Ln(NO_3)_3$. Similar behavior is observed for the titrations of $CyMe_4$-BTBP with $Ln(NO_3)_3$ (see Figure 3 for Eu^{3+} and Supporting Information).

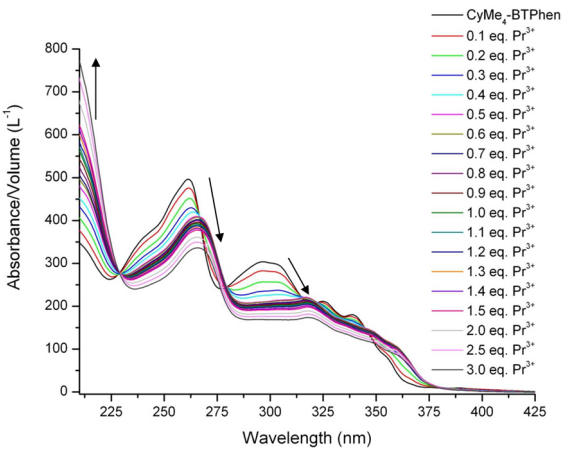

Figure 2. UV–visible absorption spectroscopic titration of $CyMe_4$-BTPhen with $Pr(NO_3)_3$ in MeOH (initial conditions, $[CyMe_4\text{-}BTPhen] = 2.0 \times 10^{-5}$ M, volume = 2.0 mL; titrant conditions, $[Pr(NO_3)_3] = 4.0 \times 10^{-4}$ M).

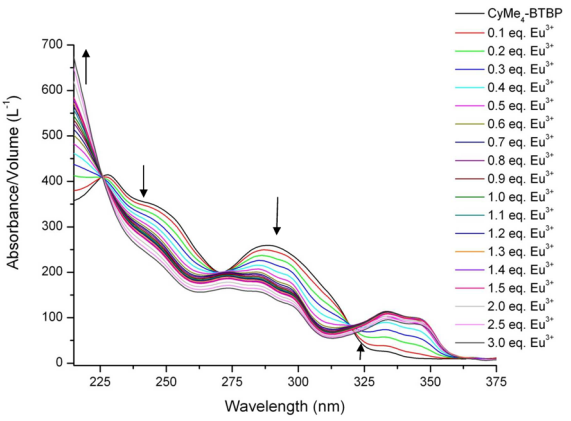

Figure 3. UV–visible absorption spectroscopic titration of $CyMe_4$-BTBP with $Eu(NO_3)_3$ in MeOH (initial conditions, $[CyMe_4\text{-}BTBP] = 2.0 \times 10^{-5}$ M, volume = 2.0 mL; titrant conditions, $[Eu(NO_3)_3] = 4.0 \times 10^{-4}$ M).

Absorption maxima at 228 and 289 nm sharply decrease in intensity with the initial addition of $Ln(NO_3)_3$ up to 0.5 equiv. Two absorption maxima are seen to emerge at 334 and 346 nm with the initial addition of $Ln(NO_3)_3$. Further additions of $Ln(NO_3)_3$ also result in a subtle decrease in the absorption intensity for most of the spectrum. Therefore, it can be deduced that the 1:2 Ln^{3+}/$CyMe_4$-BTPhen–$CyMe_4$-BTBP complex is probably most favored to form, but the 1:1 species can be forced to form in solution with excess Ln^{3+} ion present. Similar results have been previously observed for Ln^{3+} complexation behavior with analogous BTBP ligands.[26]

The overall stability constants for both 1:1 and 1:2 Ln^{3+}/$CyMe_4$-BTPhen–$CyMe_4$-BTBP species were determined by fitting the appropriate spectrophotometric titration data (Table 2). These fits confirm that the formation of both ML and ML_2 (where L is the N-donor ligand) species does occur over the

dx.doi.org/10.1021/ic301599y | Inorg. Chem. XXXX, XXX, XXX–XXX

Table 2. Fitted Metal–Ligand Overall Stability Constants Determined from UV–Visible Spectroscopic Data Using *Hyperquad*[28] (I = 0 M in MeOH; T = 25 °C)

N-donor ligand	Ln^{3+}	overall stability constant (log β_{ML}) log β_{11}	standard deviation[a]	log β_{12}	standard deviation[a]	σ^b
$CyMe_4$-BTPhen	Pr^{3+}	4.7	0.5	11.8	0.1	0.0032
	Eu^{3+}	7.9	0.5	15.6	1.0	0.0028
	Tb^{3+}	8.1	0.5	13.2	0.5	0.011
$CyMe_4$-BTBP	La^{3+}	4.4[c]	0.2[c]	8.8[c]	0.1[c]	
	Pr^{3+}	10.9	0.7	18.9	1.1	0.0042
	Eu^{3+}	9.5	0.6	16.9	1.1	0.0067
		6.5[c]	0.2[c]	11.9[c]	0.5[c]	
	Tb^{3+}	8.8	0.2	15.9	0.4	0.0037
	Yb^{3+}	5.9[c]	0.1[c]			

[a]Standard deviations determined by the fitting process. [b]Goodness-of-fit parameter. [c]Reference 27 (I = 0.01 M Et_4NNO_3; T = 25 °C; in MeOH; determined by UV–visible absorption spectroscopy).

conditions used in these titrations, as has been observed previously in similar titrations of $CyMe_4$-BTBP with La^{3+} and Eu^{3+}.[27] The speciation plots corresponding to the titrations with $CyMe_4$-BTBP (see the Supporting Information) show the initial emergence of the ML_2 species when less than 0.5 mol equiv of lanthanide is present (relative to L), with further additions of lanthanide showing the increasing formation of the ML species. The magnitude of the lanthanide stability constants for the $CyMe_4$-BTBP species indicates the greatest affinity for the mid-lanthanides with lower stability constants obtained for the lanthanides at either end of the series, which is in agreement with previous work and the corresponding distribution ratios for Ln^{3+} extractions using $CyMe_4$-BTBP and DMDOHEMA into *n*-octanol.[12,27] The speciation plots for the $CyMe_4$-BTPhen titrations (see the Supporting Information) indicate behavior different from that observed for $CyMe_4$-BTBP. For Pr^{3+}, the 1:2 Ln/$CyMe_4$-BTPhen species is favored to form, compared to the 1:1 M/L species even at relatively high metal concentrations due to a highly positive cooperative effect for the formation of the ML_2 species. However, this strong cooperative effect diminishes substantially with progress along the lanthanide series where the ML species is predominantly favored for Tb^{3+} even at reasonably low metal concentrations. The stability constants for 1:1 Ln/$CyMe_4$-BTPhen increases as the lanthanide series is traversed. The differences observed between the lanthanide stability behaviors for complexes of $CyMe_4$-BTBP and $CyMe_4$-BTPhen are most likely due to the lack of flexibility in the BTPhen backbone, resulting in the greater likelihood of a mismatch between the lanthanide ionic radius and the $CyMe_4$-BTPhen binding cavity as the lanthanide series is traversed.

The absorption spectroscopic profiles showed little difference between the light and heavy lanthanides, but XRD studies (see the Solid-State Structure section) indicate that the heavy lanthanides in the 1:2 Ln^{3+}/$CyMe_4$-BTPhen–$CyMe_4$-BTBP complexes prefer to have their coordination sphere completed by water, whereas the lighter lanthanide complexes generally prefer to have nitrate in their coordination environment, a consequence of the lanthanide contraction. This is commonly observed in a series of lanthanide complexes of a given multidentate ligand.[29] Luminescence studies were therefore undertaken in an attempt to assess the involvement of nitrate and water in the coordination sphere of these lanthanide species, as has been performed previously to investigate the coordination behavior of other extractant molecules.[30] Excitation and emission spectra of the Eu^{3+} and Tb^{3+} complexes with $CyMe_4$-BTPhen and $CyMe_4$-BTBP are displayed in Figure 4 and in the Supporting Information. Excitation into the

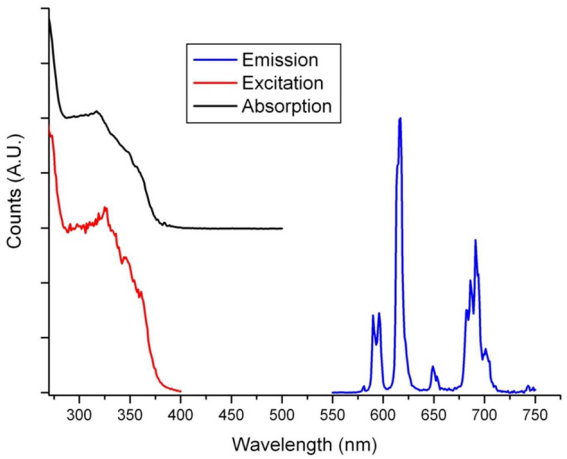

Figure 4. Emission (following excitation at 320 nm), excitation (monitoring emission at 616 nm), and absorption spectra of $[Eu(CyMe_4\text{-BTPhen})_2(X)]^{n+}$ in MeOH (X = H_2O/NO_3^-; n = 3 and 2).

intraligand absorption bands (280–330 nm) of the Eu^{3+} and Tb^{3+} complexes produced characteristic f-centered emission spectra with resolvable bands due to the $^5D_0$ to ^7F_J and $^5D_4$ to ^7F_J (J = 0–6) transitions, respectively. The emission spectrum of the Eu^{3+} complexes are dominated by the electric-dipole-allowed ΔJ = 2 transition, which is hypersensitive to the site symmetry. The absence of a hyperfine structure in this band indicates that the complexes exist as a single emissive species on the experimental time scale.[31] The emission profiles for the Eu^{3+} complexes are similar to those observed with other BTBP ligands, but in our examples, the splitting of the $^5D_0$ to $^7F_2$ transition at ~617 nm upon complexation with the N-donor ligands is not resolved, which has been observed previously in some examples.[24,32] The respective excitation spectra recorded at the emission maxima (545 nm for Tb^{3+} and 616 nm for Eu^{3+}) display ligand-centered absorption bands that overlap well with the absorption spectra, indicating that sensitized emission is occurring in all of the systems under study.

In order to assess the inner coordination sphere of the complexes, lifetime data were recorded in MeOH and MeOH-d_4 following 320 nm excitation (e.g., see Figure 5) and the number of coordinated MeOH molecules determined according to Horrock's equation (eq 1)[33]

$$q_{\text{bound MeOH}} = A\left[\left(\frac{1}{\tau_{\text{MeOH}}}\right) - \left(\frac{1}{\tau_{\text{CD}_3\text{OD}}}\right)\right] \quad (1)$$

where A is a proportionality constant; A = 2.1 ms for Eu^{3+} and A = 8.4 ms for Tb^{3+}.

For solutions of Eu^{3+} and $CyMe_4$-BTPhen in a 2:1 molar ratio, this gave a q value of 0.3; an identical q value was obtained for the analogous complex with $CyMe_4$-BTBP of 0.3 (Table 3). This strongly suggests that the first coordination sphere of the complexes is completed by ligation of nitrate

dx.doi.org/10.1021/ic301599y | Inorg. Chem. XXXX, XXX, XXX–XXX

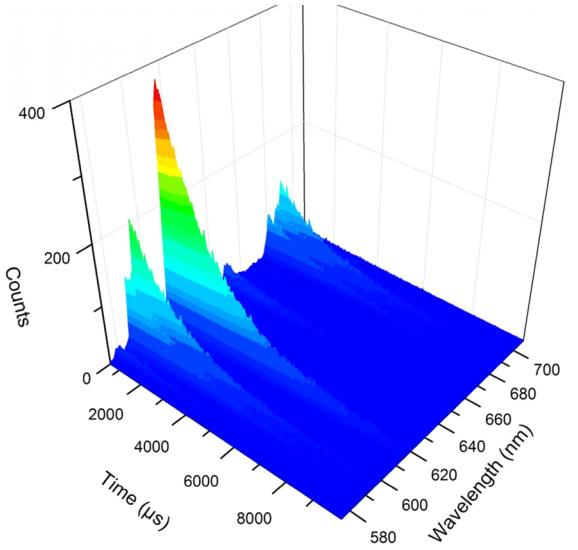

Figure 5. Time-resolved emission spectrum of $[Eu(CyMe_4\text{-}BTPhen)_2(X)]^{n+}$ in MeOH following excitation at 320 nm (X = H_2O/NO_3^-; n = 3 and 2).

Table 3. Photophysical Properties of Solutions of $Ln(NO_3)_3$ with Tetra-N-Donor Ligands in a 1:2 Molar Ratio at 298 K[a]

complex	λ_{em} (nm)	τ_{MeOH} (ms)	τ_{MeOD} (ms)	q_{MeOH}
$[Eu(BTBP)_2(X)]^{n+}$	617	1.94	2.61	0.3
$[Eu(BTPhen)_2(X)]^{n+}$	617	1.49	1.87	0.3

[a]All lifetimes were recorded by TCSPC at 320 nm excitation using a 5 W xenon flashlamp and are subject to a ±10% error. Identical data within error were obtained for 1:3 and 1:5 solutions of $Eu^{3+}/L_{N_4\text{-donor}}$ and the crystalline complexes **3** and **8**.

anions rather than exchangeable solvent molecules, and there may be a minor species that exists, with either water or MeOH occupying this coordination site for these Eu^{3+} complexes. Because the emissive quantum yield of a solvated species would be much lower, the contribution to the initial emission intensity will be low, perhaps precluding observation of a second species in solution, and/or the rate of solvent and nitrate anion exchange is much faster than the luminescence time scale, so a noninteger value of q is determined. Similar data were obtained for 1:3 and 1:5 molar ratios of Eu^{3+} with both N_4-donor ligands and the isolated complexes **3** and **8**, suggesting that the 1:2 $Ln^{3+}/L_{N_4\text{-donor}}$ complex is the only emissive species formed under these conditions.

In the case of the Tb^{3+} complexes of both ligands, excitation into the ligand absorption bands resulted in comparatively weak emission spectra. This is unsurprising given the estimated triplet energies of the ligands and the high-energy emissive $^5D_4$ excited state and suggests that back-energy transfer from the Tb^{3+} excited-state manifold to the ligand triplet state is a competitive nonradiative decay process.[34] This is corroborated by the fact that the radiative lifetimes for the Tb^{3+} emission are extremely short; the kinetic traces could be satisfactorily fitted with two exponential functions, giving lifetime values of approximately 18 and 6 μs (for solutions of BTBP in MeOH). Moreover, the kinetic traces recorded without a time gate and delay additionally exhibit a short-lived component of nanosecond order, which we attribute to ligand-centered emission.

Solid-State Structure. Single-crystal XRD studies of complexes of Tb^{3+}, Eu^{3+}, and Pr^{3+} with ligands $CyMe_4$-BTBP and $CyMe_4$-BTPhen were obtained (**1**–**4** and **6**–**10**, respectively). The complex of Yb^{3+} with $CyMe_4$-BTPhen was also studied (**5**). Complexes **3**–**5** are isostructural crystallizing in the orthorhombic space group *Fdd*2. Plots of these structures are displayed in Figures 6–11 (complexes **1**, **3**, **6**, and **8**–**10**) f6 – f11

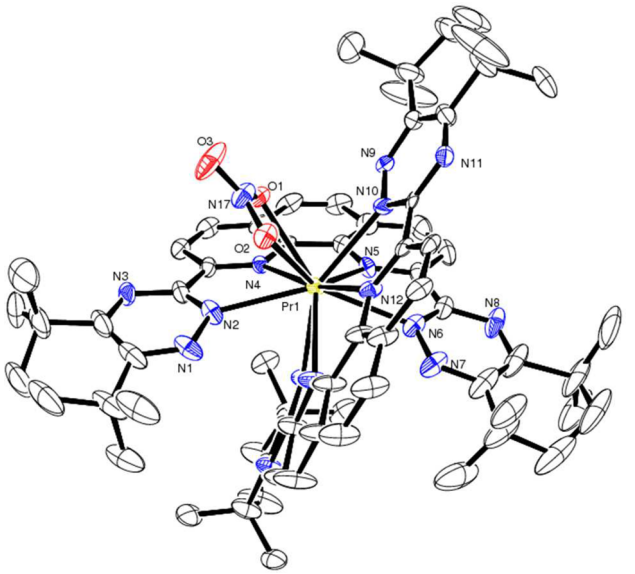

Figure 6. ORTEP plot of the complex cation of **1**, with crystallographic numbering (H atoms omitted). Probability ellipsoids of 50% displayed.

and the Supporting Information (complexes **2**, **4**, **5**, and **7**) with crystal data given in Tables 4 and 5. In the vast majority of cases (**1**–**8** and **10**), two of the N-donor ligands (either $CyMe_4$-BTBP or $CyMe_4$-BTPhen) were found to coordinate to the metal center occupying four coordination sites each, with another ligand (water or nitrate) occupying a cavity between t4t5

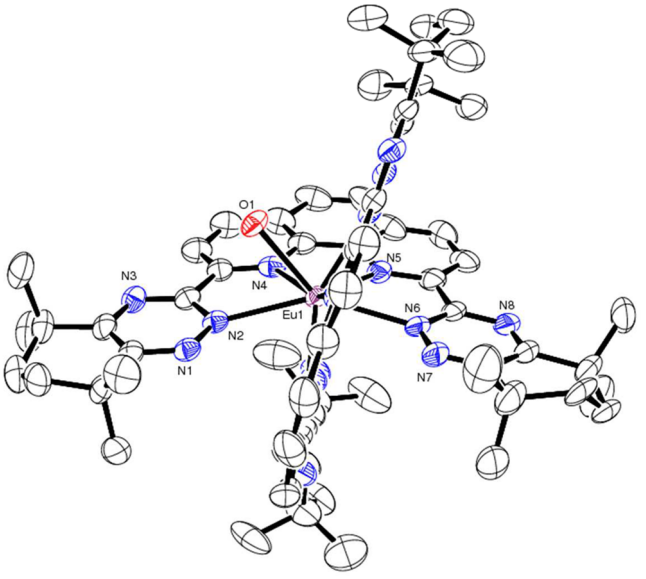

Figure 7. ORTEP plot of the complex cation of **3**, with crystallographic numbering (H atoms omitted). Probability ellipsoids of 50% displayed.

dx.doi.org/10.1021/ic301599y | Inorg. Chem. XXXX, XXX, XXX–XXX

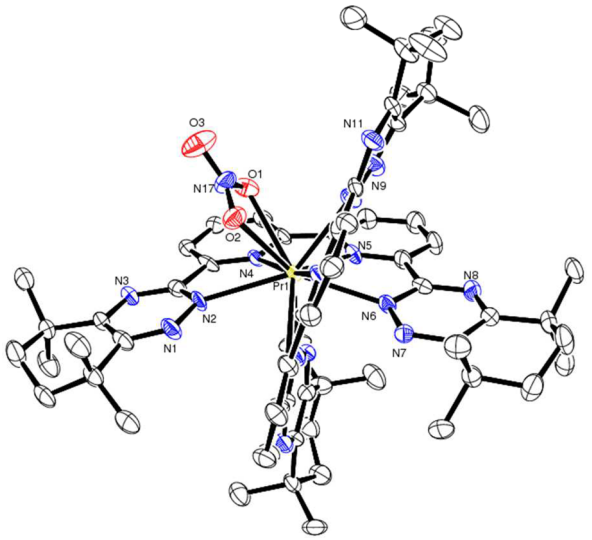

Figure 8. ORTEP plot of the complex cation of **6**, with crystallographic numbering (H atoms omitted). Probability ellipsoids of 50% displayed.

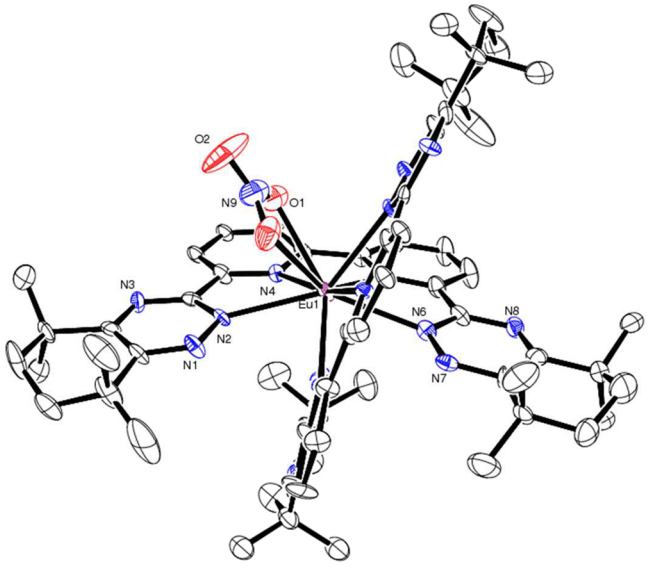

Figure 9. ORTEP plot of the complex cation of **8**, with crystallographic numbering (H atoms omitted). Probability ellipsoids of 50% displayed.

the two bound N-donor ligands, giving a distorted capped square-antiprismatic geometry about the Ln^{3+} center. This leads to a total coordination number of 9 for water-coordinated complexes (**3**–**5** and **10**) and 10 for the bidentate nitrate-coordinated complexes (**1**, **2**, and **6**–**8**).

For the Ln^{3+} complexes with $CyMe_4$-BTPhen, only 1:2 $Ln^{3+}/L_{N_4\text{-donor}}$ coordination stoichiometries have been isolated and structurally characterized in the solid state. The nitrate ion is found to occupy the remaining coordination sites in the Pr^{3+} complexes isolated, while a single water molecule completes the coordination sphere for the $CyMe_4$-BTPhen complexes of the heavier Ln^{3+} ions investigated in this study (Eu^{3+}, Tb^{3+}, and Yb^{3+} in **3**–**5**). This is likely to be due to a combined effect of the lanthanide contraction and the structural rigidity of the $CyMe_4$-BTPhen ligand sterically hindering the remaining coordination sites in the more contracted structures of Eu^{3+}, Tb^{3+}, and Yb^{3+} such that only water can access this binding cavity in these solid-state systems. However, previous work has shown that the 1:2 complex of $Eu^{3+}/CyMe_4$-BTPhen can be obtained with a nitrate ion completing the coordination sphere in the solid state where MeOH was used as the reaction solvent,[20] thus indicating that the position of the equilibrium between bound nitrate and bound water in these Ln^{3+} complexes may be influenced by the choice of solvent. The nitrate-coordinated complexes form 2+ charged complex cations, while the water-coordinated complexes form tricationic complex cations, where charge balance is achieved with nonbinding nitrate anions in the crystal lattice (**1** and **3**–**5**) or with an anionic metallonitrato species (**2**). The previously obtained $[Eu(CyMe_4\text{-BTPhen})_2(NO_3)]^{2+}$ solid-state complex was also charge-balanced with a pentanitratolanthanide anionic species.[20]

All of the M–N bond lengths in the $CyMe_4$-BTPhen-containing structures decrease as the lanthanide series is traversed from left to right (Table 6), as expected due to the lanthanide contraction. In all cases, the lanthanide ion sits outside of the plane of the N-donor ligand cavity. The out-of-plane displacement of the Ln^{3+} ion from the average plane defined by the four coordinating N atoms for each N-donor ligand follows a trend similar to that of the bond lengths by decreasing across the lanthanide series: ~0.80/0.71, 0.77/0.62, 0.56, 0.55, and 0.51 Å for species **1**–**5**, respectively. The average $M-N_{triazinyl}$ bonds lengths are consistently longer than those for the $M-N_{Phen}$ bonds in the Eu^{3+}, Tb^{3+}, and Yb^{3+} complexes (**3**–**5**). This may imply that a greater degree of interaction exists between the Ln^{3+} ion and the phenanthroline N-donor atoms than that with the triazinyl N-donor atoms. However, the same cannot be said for the structures of the Pr^{3+} complexes obtained (**1** and **2**), where in some instances the $M-N_{Phen}$ bond lengths are, in fact, longer than the $M-N_{trazinyl}$ bond distances. The previously obtained structure of $[Eu(CyMe_4\text{-BTPhen})_2(NO_3)]^{2+}$ shows little difference between the $Eu-N_{triazinyl}$ and $Eu-N_{Phen}$ bond distances.[20] Therefore, it is most likely the triazinyl groups that are restrained to be further away from the Ln^{3+} center relative to the phenanthroline backbone as the Ln center approaches the plane of the $CyMe_4$-BTPhen binding cavity, as this is only evident for the latter lanthanides. The $Ln-O_{water}$ bond distances also decrease as the lanthanide series is traversed from left to right because of lanthanide contraction (Table 6). The $Pr-O_{nitrate}$ bond distances for **1** and **2** [2.592(7) and 2.544(7) Å for **1**; 2.581(5) and 2.605(5) Å for **2**] are typical for Pr^{3+} complexes with coordinated nitrates (2.5–2.8 Å).[23,35,36]

Where $CyMe_4$-BTBP is the ligand, both 1:1 (**9**) and 1:2 $Ln^{3+}/CyMe_4$-BTBP (**6**–**8** and **10**) coordination structures were isolated. Structures of metal complexes with $CyMe_4$-BTBP have only been previously obtained for Eu^{3+}, U^{4+}, and $\{UO_2\}^{2+}$.[36,37] Previous studies of the complexation of Eu^{3+} with $CyMe_4$-BTBP, using a preparation similar to that described in this work, isolated structures consisting of the same 1:2 and 1:1 $Eu^{3+}/CyMe_4$-BTBP complexes found (structures **8** and **9**, respectively). However, these structures exhibit different crystal forms due to either different counterions or alternate solvent molecules of crystallization present in the lattices.[24] Further structural information has been obtained for Ln^{3+} complexes with C2-BTBP, where only 1:1 Ln/C2-BTBP complexes were isolated, essentially for the entire lanthanide series.[23] The remaining coordination sites were occupied by three nitrate anions to give charge-neutral species.[23] The structure of the

dx.doi.org/10.1021/ic301599y | Inorg. Chem. XXXX, XXX, XXX–XXX

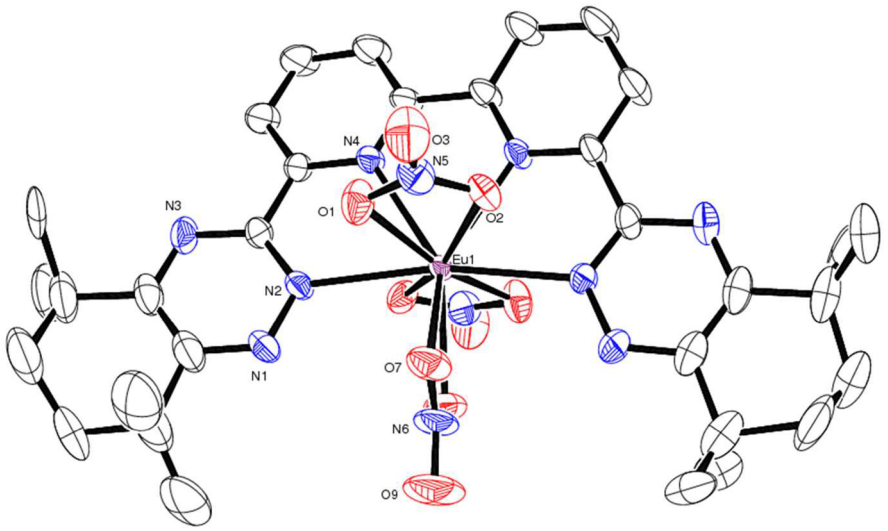

Figure 10. ORTEP plot of the complex molecule of **9**, with crystallographic numbering (H atoms omitted). Probability ellipsoids of 50% displayed.

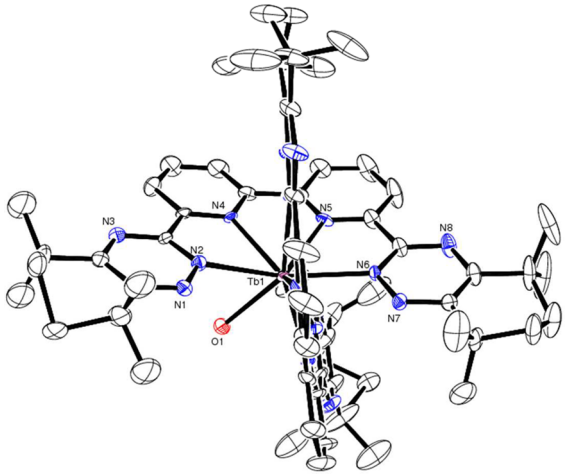

Figure 11. ORTEP plot of the complex cation of **10**, with crystallographic numbering (H atoms omitted). Probability ellipsoids of 50% displayed.

Eu^{3+} complex, **9**, is analogous to the Ln^{3+} complexes of C2-BTBP. For the cationic Ln^{3+} complexes of $CyMe_4$-BTBP, charge balance was achieved either with extra lattice nitrate anions (**6**, **8**, and **10**) or in combination with a hexanitratometallo anion (**7**). The two crystalline forms obtained from the complexation of Eu^{3+} with $CyMe_4$-BTBP offers further insight into the equilibrium between 1:1 and 1:2 Ln/BTBP−BTPhen complex stoichiometries. Although it may be possible for both of these stoichiometries to be isolated, the vast majority of the structural evidence indicates that the lanthanides preferentially coordinate to two of these tetra N-donor ligands from this class of extractant molecules. In contrast to the $CyMe_4$-BTPhen structures, metal-bound nitrate ions are observed with all $CyMe_4$-BTBP species except Tb^{3+}. This is presumably due to the greater flexibility afforded from the bipyridine, compared to the "locked" phenanthroline, permitting the sterically larger bidentate nitrate anion, relative to water, to bind to the Ln^{3+} center.

For all of the complexes of $CyMe_4$-BTBP (**6**−**10**), the Ln−N bond distances (Table 7) decrease as the lanthanide series is traversed from left to right, similar to the $CyMe_4$-BTPhen- and C2-BTBP-containing structures.[23] The $Ln-O_{nitrate}$ bond lengths also clearly decrease across the series, demonstrating lanthanide contraction again. The 1:2 Ln^{3+}/$CyMe_4$-BTBP complexes bear further similarity to those of $CyMe_4$-BTPhen with the Ln^{3+} ion located outside of the average plane of the tetra-N-donor cavity and this displacement following the same trend as that of the bond lengths, decreasing across the series: ~0.73/0.78, 0.72/0.76, 0.69, and 0.56 Å for **6**−**8** and **10**, respectively. However, the 1:1 Eu^{3+}/$CyMe_4$-BTBP complex (**9**) does effectively sit in the plane average plane of the four N-donor atoms (out-of-plane displacement ~0 Å). The coordination bond lengths and motifs observed in the structures of the 1:1 and 1:2 Eu^{3+}/$CyMe_4$-BTBP complexes (**8** and **9**) are similar to those observed for the structures obtained previously for the same complex molecules but in different crystal forms.[24] There is little difference observed in the Ln−N bond lengths between the 1:1 and 1:2 Ln^{3+}/BTBP complex molecular species obtained here and elsewhere,[23] suggesting that if there are indeed any cooperative or destructive effects for 1:2 Ln^{3+}/Cy-Me_4-BTBP binding over the 1:1 Ln^{3+}/Cy-Me_4-BTBP complex, they do not significantly alter the N-donor coordination environment. In contrast to the $CyMe_4$-BTPhen structures, there is no clearly identifiable trend between the $M-N_{bipy}$ and $M-N_{triazinyl}$ bond lengths for all of the $CyMe_4$-BTBP complexes. This suggests that the greater flexibility of the bipyridyl group, relative to the phenanthroline group, allows minimal distinction between the triazinyl and bipyridyl N atoms when coordinated to a Ln^{3+} ion.

XAS of Lanthanide-Extracted Species. XAS spectra were obtained for Eu^{3+} and Tb^{3+} species formed by extraction from an acidic aqueous phase into an organic phase containing an excess of either $CyMe_4$-BTBP or $CyMe_4$-BTPhen in cyclohexanone as a guide for speciation in a potential SANEX process. Studies were also performed for potential GANEX-like systems where the organic phase also included 30% TBP. XAS spectra were obtained for the crystallographically characterized solids $[Eu(CyMe_4\text{-BTPhen})_2(H_2O)]^{3+}$ (**3**) and $[Tb(CyMe_4\text{-BTPhen})_2(H_2O)]^{3+}$ (**4**) for comparative purposes. The spectra obtained show little difference between the extracted species with or without the presence of TBP (Figures 11 and 12 and the Supporting Information). This indicates that the presence of TBP does not influence lanthanide speciation when used in a

dx.doi.org/10.1021/ic301599y | Inorg. Chem. XXXX, XXX, XXX−XXX

Table 4. Crystal Data for Complexes 1−5

	[Pr(CyMe$_4$-BTPhen)$_2$(NO$_3$)](NO$_3$)$_2$·10H$_2$O (**1**)	[Pr(CyMe$_4$-BTPhen)$_2$(NO$_3$)][Pr(NO$_3$)$_5$]·1.63EtOH·0.75H$_2$O (**2**)	[Eu(CyMe$_4$-BTPhen)$_2$(H$_2$O)](NO$_3$)$_3$·9H$_2$O (**3**)	[Tb(CyMe$_4$-BTPhen)$_2$(H$_2$O)](NO$_3$)$_3$·9H$_2$O (**4**)	[Yb(CyMe$_4$-BTPhen)$_2$(H$_2$O)](NO$_3$)$_3$·9H$_2$O (**5**)
formula	$C_{68}H_{96}N_{19}O_{19}Pr$	$C_{71.25}H_{87.25}N_{22}O_{20.38}Pr_2$	$C_{68}H_{96}N_{19}O_{19}Eu$	$C_{68}H_{96}N_{19}O_{19}Tb$	$C_{68}H_{96}N_{19}O_{19}Yb$
M	1624.55	1859.70	1615.44	1642.56	1656.68
cryst syst	monoclinic	triclinic	orthorhombic	orthorhombic	orthorhombic
a (Å)	31.654(5)	13.716(5)	31.172(3)	31.3486(7)	31.3257(13)
b (Å)	26.271(5)	15.221(5)	38.128(3)	38.0261(9)	37.709(2)
c (Å)	19.501(5)	20.359(5)	14.8296(13)	14.8414(3)	14.8783(7)
α (deg)	90	107.225(5)	90	90	90
β (deg)	109.504(5)	99.422(5)	90	90	90
γ (deg)	90	97.083(5)	90	90	90
space group	*C*2/*c*	*P*$\bar{1}$	*Fdd*2	*Fdd*2	*Fdd*2
Z	8	2	8	8	8
T (K)	100(2)	100(2)	100(2)	100(2)	100(2)
μ (mm^{-1})	0.719	1.309	0.782	0.870	1.135
reflns measd	20981	25422	32709	49820	8497
reflns obsd	6002	14178	8290	9044	5110
R1 (obsd)	0.0551	0.0547	0.0512	0.0513	0.0658
wR2 (all data)	0.1257	0.1393	0.1364	0.1423	0.1984

Table 5. Crystal Data for Complexes 6−10

	[Pr(CyMe$_4$-BTBP)$_2$(NO$_3$)](NO$_3$)$_2$·4EtOH·H$_2$O (**6**)	[Pr(CyMe$_4$-BTBP)$_2$(NO$_3$)]$_2$[Pr(NO$_3$)$_6$](NO$_3$)·6CH$_3$CN (**7**)	[Eu(CyMe$_4$-BTBP)$_2$(NO$_3$)](NO$_3$)$_2$·4EtOH·2H$_2$O (**8**)	[Eu(CyMe$_4$-BTBP)(NO$_3$)$_3$]·toluene (**9**)	[Tb(CyMe$_4$-BTBP)$_2$(H$_2$O)](NO$_3$)$_3$·4EtOH (**10**)
formula	$C_{72}H_{102}N_{19}O_{14}Pr$	$C_{140}H_{166}N_{47}O_{27}Pr_3$	$C_{72}H_{104}N_{19}O_{15}Eu$	$C_{46}H_{54}N_{11}O_9Eu$	$C_{72}H_{102}N_{19}O_{14}Tb$
M	1598.64	3361.93	1627.70	1056.96	1614.63
cryst syst	monoclinic	monoclinic	orthorhombic	monoclinic	monoclinic
a (Å)	24.2790(7)	16.604(2)	16.4128(6)	26.385(2)	30.5621(7)
b (Å)	16.5467(4)	28.1161(19)	23.8916(6)	11.6674(11)	14.8217(4)
c (Å)	19.4601(5)	17.7385(14)	19.7838(6)	15.7469(14)	23.9083(6)
α (deg)	90	90	90	90	90
β (deg)	90.355(3)	106.609(10)	90	90.6730(10)	129.4280(10)
γ (deg)	90	90	90	90	90
space group	*P*2$_1$/*c*	*P*2$_1$/*n*	*Pccn*	*C*2/*c*	*C*2/*c*
Z	4	2	4	4	4
T (K)	100(2)	100(2)	100(2)	100(2)	100(2)
μ (mm^{-1})	0.697	0.988	0.884	1.359	4.723
reflns measd	77969	17453	47979	17887	25718
reflns obsd	13767	17454	6854	4618	7271
R1 (obsd)	0.0562	0.0766	0.1158	0.0430	0.0915
wR2 (all data)	0.1435	0.2209	0.2628	0.1164	0.2381

potential GANEX process with CyMe$_4$-BTBP or CyMe$_4$-BTPhen. The XAS profiles for the directly synthesized solid species (**3** and **4**) also correlate well with the corresponding extracted species (Figures 12 and 13), suggesting that the [Ln(CyMe$_4$-BTPhen)$_2$(H$_2$O)]$^{2+}$ coordination species found in the solid state also exists in the bulk organic-phase postextraction.

The shells used to fit the EXAFS data for all samples were derived from the corresponding Ln^{III} structures that have two CyMe$_4$-BTX (X = BP, Phen) ligands bound to the metal. The dominant scatter paths include a shell corresponding to the 8 N atoms from the CyMe$_4$-BTX ligands that are coordinated to the metal (∼2.51 Å) and two shells from the 16 C/N and 16 C atoms located at the ortho and meta positions relative to the coordinating N atoms, respectively (Figure 14). The initial positions of these modeled shells, relative to the central Ln atom, are averaged from the atomic positions obtained from the crystal structures determined by XRD and are located at ∼2.51, 3.42, and 4.75 Å from the Ln atom for the 8 N, 16 C/N, and 16 C shells, respectively (Figure 4 and Tables 8 and 9). It was

dx.doi.org/10.1021/ic301599y | Inorg. Chem. XXXX, XXX, XXX−XXX

Table 6. Selected Interatomic Distances (Å) for $CyMe_4$-BTPhen-Containing Complexes 1−5[a]

bond	origin	1 (Pr)	2 (Pr)	3 (Eu)	4 (Tb)	5 (Yb)
N2−M	$N_{triazinyl}$	2.636(9)	2.644(6)	2.539(5)	2.527(5)	2.475(9)
N6−M		2.623(9)	2.635(6)	2.542(5)	2.516(5)	2.507(11)
N10−M		2.623(9)	2.568(6)	N/A	N/A	N/A
N14−M		2.618(8)	2.592(6)	N/A	N/A	N/A
N4−M	N_{phen}	2.668(8)	2.632(6)	2.507(5)	2.485(5)	2.422(11)
N5−M		2.644(9)	2.587(6)	2.523(5)	2.499(5)	2.442(10)
N12−M		2.675(8)	2.617(6)	N/A	N/A	N/A
N13−M		2.638(9)	2.583(6)	N/A	N/A	N/A
O1−M	O_{water}	N/A	N/A	2.414(6)	2.398(6)	2.373(11)
O1−M	$O_{nitrate}$	2.592(7)	2.581(5)	N/A	N/A	N/A
O2−M		2.544(7)	2.605(5)	N/A	N/A	N/A

[a]N/A = not applicable. The designated bond length does not exist or is symmetry-related to another bond length.

Table 7. Selected Interatomic Distances (Å) for $CyMe_4$-BTBP-Containing Complexes 6−10[a]

bond	origin	6 (Pr)	7 (Pr)	8 (Eu)	9 (Eu)	10 (Tb)
N2−M	$N_{triazinyl}$	2.637(5)	2.654(9)	2.565(9)	2.533(4)	2.516(6)
N6−M		2.597(5)	2.595(9)	2.578(10)	N/A	2.512(6)
N10−M		2.611(5)	2.579(9)	N/A	N/A	N/A
N14−M		2.634(6)	2.597(9)	N/A	N/A	N/A
N4−M	N_{bipy}	2.638(5)	2.645(9)	2.569(8)	2.545(4)	2.485(5)
N5−M		2.623(5)	2.663(10)	2.562(9)	N/A	2.504(6)
N12−M		2.615(5)	2.650(9)	N/A	N/A	N/A
N13−M		2.633(5)	2.684(9)	N/A	N/A	N/A
O1−M	O_{water}	N/A	N/A	N/A	N/A	2.407(8)
O1−M	$O_{nitrate}$	2.596(5)	2.606(8)	2.564(10)	2.548(4)	N/A
O2−M		2.607(5)	2.625(8)	N/A	2.487(3)	N/A
O7−M		N/A	N/A	N/A	2.455(4)	N/A

[a]N/A = not applicable. The designated bond length does not exist or is symmetry-related to another bond length.

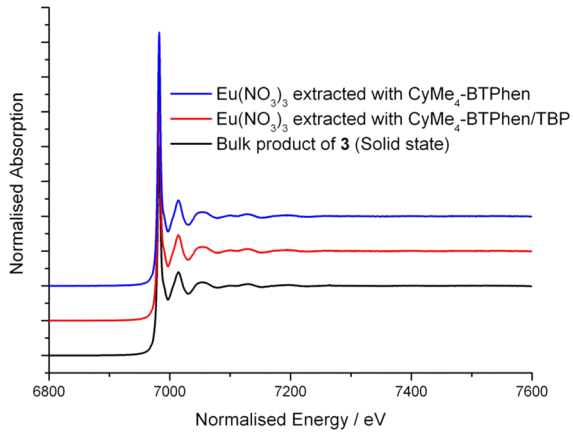

Figure 12. Eu L_{III}-edge XAS spectra of $CyMe_4$-BTPhen-containing species.

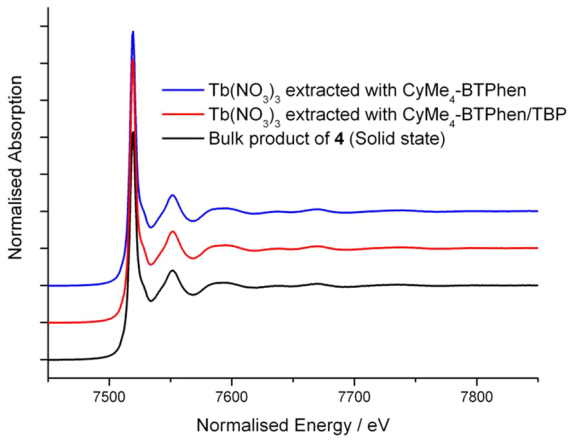

Figure 13. Tb L_{III}-edge XAS spectra of $CyMe_4$-BTPhen-containing species.

found necessary to include an extra shell assigned to 32 C/N atoms, initially located at ∼3.40 Å from the Ln atom, due to multiple scattering from the planar aromatic rings in the N-donor ligands in order to obtain appropriate fits (Figure 14). A shell corresponding to oxygen coordination at the ninth site was included in all fits, initially located at 2.4−2.6 Å from the Ln atom. Two sets of models corresponding to nitrate coordination (i.e., O shell occupancy = 2) and water coordination (i.e., O shell occupancy = 1) to the lanthanide ion were used to fit all EXAFS data in order to ascertain whether XAS can be used to distinguish between nitrate and water binding in these systems (Tables 8 and 9; see the

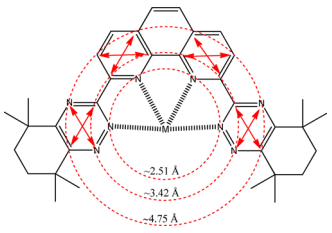

Figure 14. Depiction of the shell occupancy of complexes formed with $CyMe_4$-BTPhen (or $CyMe_4$-BTBP). Also depicted with arrows are some of the multiple scatter paths within the complex.

dx.doi.org/10.1021/ic301599y | Inorg. Chem. XXXX, XXX, XXX−XXX

Table 8. Eu L_{III}-Edge EXAFS Data[a]

physical state	aqueous phase	organic-phase extractants	chemical composition used in fitted models	occupancy[b]	interatomic distances from XRD (Å)	fitted interatomic distances[c] (Å)	σ^2 (Å^2)[d]	r[e]
solution	$Eu(NO_3)_3$	$CyMe_4$-BTBP	$[Eu(CyMe_4\text{-}BTBP)_2(NO_3)]^{2+}$	Eu−O2	2.56	2.46	0.00200	0.0159
				Eu−N8	2.57	2.59	0.00391	
				Eu−C/N16	3.44	3.44	0.00731	
				Eu−C/N32[f]	3.67	3.68	0.00791	
				Eu−C/N16	4.78	4.87	0.00374	
solution	$Eu(NO_3)_3$	$CyMe_4$-BTBP + TBP	$[Eu(CyMe_4\text{-}BTBP)_2(NO_3)]^{2+}$	Eu−O2	2.56	2.55	0.00567	0.0193
				Eu−N8	2.57	2.55	0.00594	
				Eu−C/N16	3.44	3.45	0.00632	
				Eu−C/N32[f]	3.67	3.66	0.00796	
				Eu−C/N16	4.78	4.87	0.00554	
solution	$Eu(NO_3)_3$	$CyMe_4$-BTPhen	$[Eu(CyMe_4\text{-}BTPhen)_2(NO_3)]^{2+}$	Eu−O2		2.60	0.00200	0.0206
				Eu−N8	2.51	2.55	0.00493	
				Eu−C/N16	3.41	3.45	0.00496	
				Eu−C/N32[f]	3.65	3.69	0.00800	
				Eu−C/N16	4.75	4.91	0.00303	
solution	$Eu(NO_3)_3$	$CyMe_4$-BTPhen + TBP	$[Eu(CyMe_4\text{-}BTPhen)_2(NO_3)]^{2+}$	Eu−O2		2.58	0.00432	0.0222
				Eu−N8	2.51	2.56	0.00486	
				Eu−C/N16	3.41	3.45	0.00484	
				Eu−C/N32[f]	3.65	3.69	0.00800	
				Eu−C/N16	4.75	4.91	0.00282	
solid	N/A	N/A	$[Eu(CyMe_4\text{-}BTPhen)_2(H_2O)]^{3+}$	Eu−O1	2.41	2.57	0.00121	0.0273
				Eu−N8	2.51	2.56	0.00504	
				Eu−C/N16	3.41	3.44	0.00663	
				Eu−C/N32[f]	3.65	3.68	0.00800	
				Eu−C/N16	4.75	4.92	0.00944	
			$[Eu(CyMe_4\text{-}BTPhen)_2(NO_3)]^{2+}$	Eu−O2		2.56	0.00193	0.0231
				Eu−N8	2.51	2.56	0.00667	
				Eu−C/N16	3.41	3.43	0.00605	
				Eu−C/N32[f]	3.65	3.68	0.00800	
				Eu−C/N16	4.75	4.91	0.00763	

[a] S_0^2 is fitted but constrained to be within the range of 0.8−1.0 and the same value for all shells. [b] Occupancy numbers, held constant at given values. [c] ±0.02 Å. [d] Debye−Waller factors. [e] Parameter describing goodness of fit = weighted sum of squares of residuals divided by the degree of freedom. [f] Shell due to multiple scattering.

Supporting Information). The EXAFS data fits were obtained by allowing the shell distances to be refined, while the shell occupancies were fixed at chosen integer values. Attempts were made to fit the EXAFS data to a model corresponding to the coordination of one molecule of $CyMe_4$-BTX with three nitrate molecules occupying the remaining coordination sites, but these did not give any statistically justifiable fits.

Fits for all of the EXAFS data obtained, using a model relating to the coordination of two $CyMe_4$-BTX molecules, gave very good statistical correlations (Figure 15 and Tables 8 and 9; see the Supporting Information), indicating that the predominant lanthanide species in the bulk organic phase formed by extraction with these tetra-N-donor molecules is a 1:2 $Ln^{3+}/CyMe_4$-BTX complex. The refined radial distances for the three closest N-donor ligand-based shells to the Ln center

dx.doi.org/10.1021/ic301599y | Inorg. Chem. XXXX, XXX, XXX−XXX

Table 9. Tb L_{III}-Edge EXAFS Data[a]

physical state	aqueous phase	organic-phase extractants	chemical composition used in fitted models	occupancy[b]	interatomic distances from XRD (Å)	fitted interatomic distances (Å)[c]	σ^2 (Å^2)[d]	r[e]
solution	$Tb(NO_3)_3$	$CyMe_4$-BTBP	$[Tb(CyMe_4\text{-}BTBP)_2(NO_3)]^{2+}$	Tb−O2		2.53	0.00347	0.0140
				Tb−N8	2.50	2.51	0.00654	
				Tb−C/N16	3.38	3.39	0.00530	
				Tb−C/N32[f]	3.61	3.65	0.00800	
				Tb−C/N16	4.72	4.83	0.00165	
solution	$Tb(NO_3)_3$	$CyMe_4$-BTBP + TBP	$[Tb(CyMe_4\text{-}BTBP)_2(NO_3)]^{2+}$	Tb−O2		2.52	0.00365	0.0146
				Tb−N8	2.50	2.51	0.00675	
				Tb−C/N16	3.38	3.40	0.00576	
				Tb−C/N32[f]	3.61	3.64	0.00800	
				Tb−C/N16	4.72	4.83	0.00160	
solution	$Tb(NO_3)_3$	$CyMe_4$-BTPhen	$[Tb(CyMe_4\text{-}BTPhen)_2(NO_3)]^{2+}$	Tb−O2		2.52	0.00210	0.0133
				Tb−N8	2.52	2.52	0.00840	
				Tb−C/N16	3.40	3.40	0.00570	
				Tb−C/N32[f]	3.62	3.66	0.00800	
				Tb−C/N16	4.73	4.84	0.00190	
solution	$Tb(NO_3)_3$	$CyMe_4$-BTPhen + TBP	$[Tb(CyMe_4\text{-}BTPhen)_2(NO_3)]^{2+}$	Tb−O2		2.53	0.00204	0.0134
				Tb−N8	2.52	2.51	0.00835	
				Tb−C/N16	3.40	3.40	0.00537	
				Tb−C/N32[f]	3.62	3.66	0.00800	
				Tb−C/N16	4.73	4.84	0.00185	
solid	N/A	N/A	$[Tb(CyMe_4\text{-}BTPhen)_2(H_2O)]^{3+}$	Tb−O1	2.40	2.54	0.00196	0.0166
				Tb−N8	2.52	2.52	0.00620	
				Tb−C/N16	3.40	3.41	0.00601	
				Tb−C/N32[f]	3.62	3.66	0.00800	
				Tb−C/N16	4.73	4.85	0.00532	
			$[Tb(CyMe_4\text{-}BTPhen)_2(NO_3)]^{2+}$	Tb−O2		2.53	0.00199	0.0141
				Tb−N8	2.52	2.52	0.00772	
				Tb−C/N16	3.40	3.40	0.00529	
				Tb−C/N32[f]	3.62	3.66	0.00800	
				Tb−C/N16	4.73	4.84	0.00324	

[a] S_0^2 is fitted but constrained to be within the range of 0.8−1.0 and the same value for all shells. [b] Occupancy numbers, held constant at given values. [c] ±0.02 Å. [d] Debye−Waller factors. [e] Parameter describing goodness of fit = weighted sum of squares of residuals divided by the degree of freedom. [f] Shell due to multiple scattering.

(i.e., 8 N, 16 C/N, and 32 C/N shells) generally only show minimal shifts from the initial input values derived from the structural information obtained by XRD (Tables 8 and 9; see the Supporting Information). The radial distance of the 16 C shell does typically refine to a slightly larger value (4.80−4.95 Å) relative to the initial input value (4.70−4.80 Å) for the extracted solutions and solid-state samples. This suggests that either this outer C shell is influenced by multiple scattering effects or some fluctuation of the N_4-donor ligand occurs at the outer regions of these lanthanide complexes. No significant differences in the refined radial distances are observed in the extracted samples when TBP is present or not, providing further proof that TBP that does not influence Ln^{3+} speciation in a GANEX process with $CyMe_4$-BTX and TBP in the organic phase.

dx.doi.org/10.1021/ic301599y | Inorg. Chem. XXXX, XXX, XXX−XXX

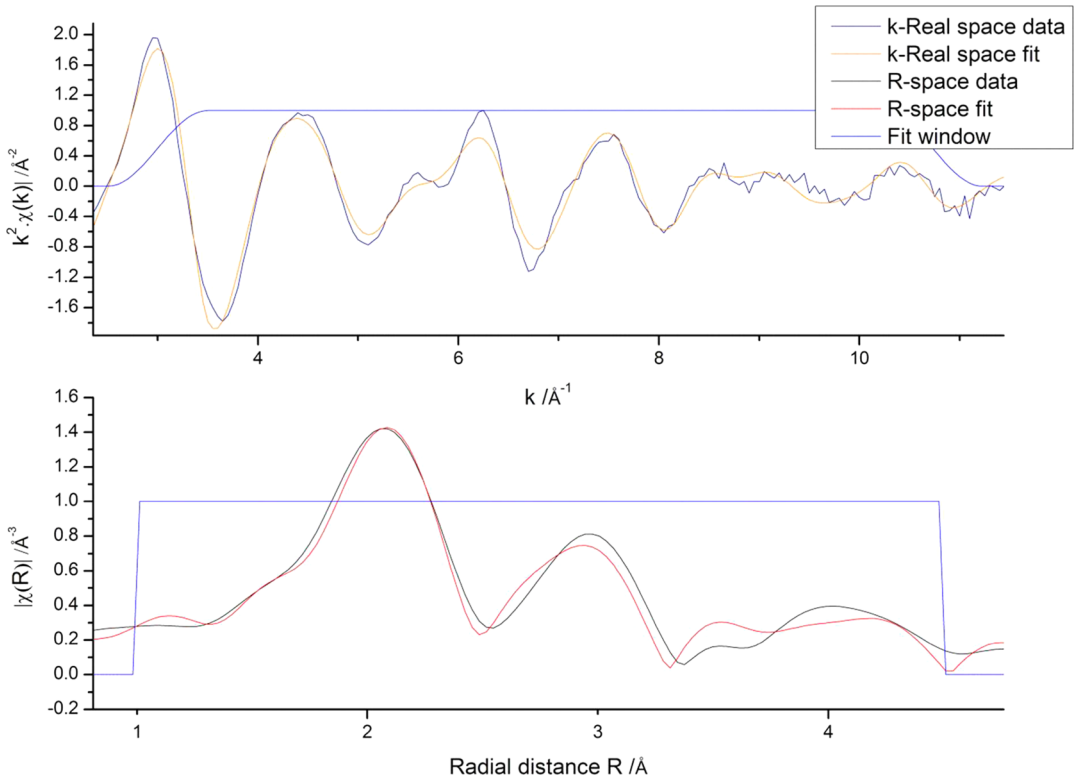

Figure 15. Eu L_{III}-edge EXAFS spectrum in *k* space (upper plot) and its Fourier transform in *R* space (lower plot) of the extraction of $Eu(NO_3)_3$ (10 mM) from an aqueous solution (1 M HNO_3 and 3 M $NaNO_3$) into cyclohexanone with $CyMe_4$-BTPhen (50 mM). The data are fitted to the model complex $[Eu(CyMe_4\text{-BTPhen})_2(NO_3)]^{2+}$.

The identity of the ninth coordination site species cannot be unambiguously assigned from the EXAFS data because the fits are unable to resolve the relatively small change between nitrate and water coordination at this site. Both sets of models, either with water or nitrate bound at the ninth coordination site, provided fits with very good statistical correlations (Tables 8 and 9; see the Supporting Information). The fits for all of the Eu L_{III}-edge data (Table 8; see the Supporting Information) show that the first O shell refines to give Eu−O distances between 2.46 and 2.60 Å. There is little distinction between the refined Eu−O distances when the shell occupancy is fixed at 1 (for water coordination) or 2 (for nitrate coordination). The refined Eu−$O_{nitrate}$ distances agree with those bond lengths determined for structures **8** [2.56(1) Å] and **9** [2.548(4) Å] and fall within the range of all known Eu−$O_{nitrate}$ distances (2.31−2.82 Å) established by crystallography.[35,38] The refined Eu−O_{water} distances also fall within the wide range of Eu−O_{water} bond lengths from previously reported structures (2.27−2.72 Å)[35,39] but are larger than this distance in complex **3** [2.414(6) Å]. The O shells for all of the Tb L_{III}-edge EXAFS spectra modeled with either water or nitrate coordination (Table 9; see the Supporting Information) all refine to within a narrow range of 2.52−2.54 Å from the Tb center and fall within the relatively wide range of known Tb−$O_{nitrate}$ (2.19−2.85 Å)[35,40] and Tb−O_{water} bond lengths (2.27−2.70 Å).[35,39] As is similarly observed in the equivalent europium studies, all of the Tb−O_{water} distances refined from the EXAFS data are larger than that observed in complex **4** [2.397(6) Å] by XRD. The refined radial distances for these low-occupancy O shells generally match the refined location for the dominant 8 N shell from the coordinating N-donor ligands even when these distances are expected to be different. This is particularly evident in the EXAFS fits of complexes **3** and **4** in the solid state, which have also been characterized by XRD. The refined distances for the O shells obtained from the fits of the EXAFS data in these solid-state samples (Eu−O for **3** = 2.57 Å; Tb−O for **4** = 2.54 Å) are distinctly longer than those observed by XRD [Eu−O for **3** = 2.414(6) Å; Tb−O for **4** = 2.397(6) Å] and are similar to the refined radial distances of the 8 N shell (Eu−N for **3** = 2.56 Å; Tb−N for **4** = 2.52 Å). It may be that the high-occupancy 8 N shell is masking the contribution of the lower-occupancy (1 or 2) O shell.

EXPERIMENTAL SECTION

General Procedures. Elemental analyses were performed with a Carlo Erba Instruments CHNS-O EA1108 elemental analyzer for carbon, hydrogen, and nitrogen and a Fisons Horizon elemental analysis ICP-OES spectrometer for praseodymium, europium, and terbium. ESI-MS (positive ion) was performed using a Micromass Platform spectrometer. Solution UV−visible spectra were recorded on a PG Instruments T60U spectrophotometer with a fixed spectral bandwidth of 2 nm. Typical scan ranges were 200−500 nm at a scan rate of ~390 nm min^{-1}. Excitation and emission spectra were recorded with Edinburgh Instrument FP920 phosphorescence lifetime spectrometer equipped with a 5 W microsecond-pulsed xenon flashlamp (with single 300 mm focal length excitation and emission monochromators in a Czerny Turner configuration) and a red-sensitive photomultiplier in Peltier (air-cooled) housing (Hamamatsu R928P) using a gate time of 0.05 ms and a delay time of 0.5 ms. Excitation spectra were obtained using the following emission wavelengths: Eu^{3+}, 616 nm; Tb^{3+}, 545 nm. Lifetime data were recorded following 320 nm excitation with a microsecond-pulsed xenon flashlamp (Edinburgh Instruments) using the multichannel scaling method. Lifetimes were obtained by a tail fit on the data obtained, and the quality of the fit was judged by minimization of reduced χ^2 and residuals squared. Where the decay profiles are

dx.doi.org/10.1021/ic301599y | *Inorg. Chem.* XXXX, XXX, XXX−XXX

reported as monoexponential, fitting to a double-exponential decay yielded no improvement in the fit, as judged by minimization of residuals squared and reduced χ^2.

Syntheses and Solution Preparations. All chemicals were purchased from Sigma Aldrich and were used as supplied. $CyMe_4$-BTPhen and $CyMe_4$-BTBP were synthesized as previously described[20,23] but using an improved purification methodology.

Purification of $CyMe_4$-BTPhen and $CyMe_4$-BTBP. The crude product of $CyMe_4$-BTPhen or $CyMe_4$-BTBP was dissolved in DCM and loaded onto a column of silica resin. The column was washed with neat DCM, quickly eluting a yellow solution and leaving a dark-orange/brown band at the top of the column. The solvent was removed from the yellow eluent by rotary evaporation, yielding a vibrant-yellow powder, which was found to be pure by NMR spectroscopy. The purified product was found to be soluble in DCM, cyclohexanone, and 1-octanol up to concentrations of 5 mM. Further purified $CyMe_4$-BTPhen/$CyMe_4$-BTBP could be obtained by elution with 1−5% (v/v) MeOH in DCM from the silica column.

Synthesis of Pr^{3+} Complexes with $CyMe_4$-BTPhen. A solution of $Pr(NO_3)_3{\cdot}6H_2O$ (23 mg, 54 μmol) in CH_3CN (5 mL) was added to a solution of $CyMe_4$-BTPhen (30 mg, 54 μmol) in DCM (5 mL) and left standing to evaporate to dryness. The resultant powder was dissolved in a mixture of CH_3CN (2 mL), DCM (2 mL), and EtOH (0.5 mL) and again allowed to evaporate slowly in order to crystallize. A yellow platelike crystal was selected from the isolated material, and XRD analysis indicated that the composition of the crystal was of the formulation $[Pr(CyMe_4\text{-}BTPhen)_2(NO_3)](NO_3)_2{\cdot}10H_2O$ (**1**·$10H_2O$). Elemental analysis of the isolated material indicated that the composition of the bulk product was of the formulation $[Pr(CyMe_4\text{-}BTPhen)_2(NO_3)][Pr(NO_3)_5]{\cdot}2H_2O$ (**2**·$2H_2O$). Elem anal. Calcd for $[(C_{34}H_{38}N_8)_2(NO_3)Pr][(NO_3)_5Pr]{\cdot}2H_2O$: C, 45.19; H, 4.46; N, 17.05; Pr, 15.59. Found: C, 45.01; H, 4.08; N, 16.90; Pr, 15.23. The bulk material was dissolved in EtOH (1 mL) and allowed to slowly evaporate over 1 week, yielding yellow blocklike crystals suitable for single-crystal XRD analysis (yield = 0.03 g). ESI-MS (positive ion): m/z 659 ($[[(C_{34}H_{38}N_8)_2(NO_3)Pr]^{2+}$). UV−visible spectrum (MeOH) [λ_{max}/nm (ε_{max}/L mol^{-1} cm^{-1})]: 266 (71000), 321 (38000).

Synthesis of $[Eu(CyMe_4\text{-}BTPhen)_2(H_2O)](NO_3)_3{\cdot}2H_2O$ (3·$2H_2O$). A solution of $Eu(NO_3)_3{\cdot}6H_2O$ (24 mg, 54 μmol) in CH_3CN (5 mL) was added to a solution of $CyMe_4$-BTPhen (30 mg, 54 μmol) in DCM (5 mL) and left standing to evaporate to dryness. The resultant powder was dissolved in a mixture of CH_3CN (2 mL), DCM (2 mL), and EtOH (0.5 mL) and allowed to evaporate slowly, yielding yellow blocklike crystals suitable for single-crystal XRD analysis (yield = 0.02 g). Elem anal. Calcd for $[(C_{34}H_{38}N_8)_2(H_2O)Eu](NO_3)_3{\cdot}2H_2O$: C, 54.11; H, 5.48; N, 17.63; Eu, 10.07. Found: C, 54.18; H, 5.07; N, 17.61; Eu, 10.51. ESI-MS (positive ion): m/z 666 ($[[(C_{34}H_{38}N_8)_2(NO_3)Eu]^{2+}$). UV−visible spectrum (MeOH) [λ_{max}/nm (ε_{max}/L mol^{-1} cm^{-1})]: 266 (99000), 321 (52000).

Synthesis of $[Tb(CyMe_4\text{-}BTPhen)_2(H_2O)](NO_3)_3{\cdot}H_2O$ (4·H_2O). The synthesis was performed as described for **2** except using $Tb(NO_3)_3{\cdot}5H_2O$ (17 mg, 38 μmol) and $CyMe_4$-BTPhen (21 mg, 38 μmol) as the initial reagents. Yellow platelike crystals suitable for single-crystal XRD analysis were obtained (yield = 0.02 g). Elem anal. Calcd for $[(C_{34}H_{38}N_8)_2(H_2O)Tb](NO_3)_3{\cdot}H_2O$: C, 54.51; H, 5.38; N, 17.76; Tb, 10.61. Found: C, 54.69; H, 5.17; N, 17.73; Tb, 9.82. ESI-MS (positive ion): m/z 669 ($[[(C_{34}H_{38}N_8)_2(NO_3)Tb]^{2+}$). UV−visible spectrum (MeOH) [λ_{max}/nm (ε_{max}/L mol^{-1} cm^{-1})]: 265 (96000), 322 (51000).

Synthesis of $[Yb(CyMe_4\text{-}BTPhen)_2(H_2O)](NO_3)_3{\cdot}3H_2O$ (5·$3H_2O$). The synthesis was performed as described for **2** except using $Yb(NO_3)_3{\cdot}5H_2O$ (24 mg, 54 μmol) and $CyMe_4$-BTPhen (30 mg, 54 μmol) as the initial reagents. Yellow rhombohedron-like crystals suitable for single-crystal XRD analysis were obtained (yield < 0.01 g). ESI-MS (positive ion): m/z 677 ($[[(C_{34}H_{38}N_8)_2(NO_3)Yb]^{2+}$).

Synthesis of Ln^{3+} Complexes with $CyMe_4$-BTBP. A solution of $CyMe_4$-BTBP (30 mg, 56 μmol) in DCM (1 mL) was added to a solution of $Ln(NO_3)_3{\cdot}xH_2O$ [$Pr(NO_3)_3{\cdot}6H_2O$, 12 mg, 28 μmol; $Eu(NO_3)_3{\cdot}6H_2O$, 13 mg, 28 μmol; $Tb(NO_3)_3{\cdot}5H_2O$, 12 mg, 28 μmol] in MeOH (1 mL). CH_3CN (1.5 mL) was added to the reaction mixture, and the solution was allowed to evaporate to dryness. Once dry, toluene (1.25 mL), EtOH (1.25 mL), ^{i}PrOH (1.25 mL), and DCM (1.25 mL) were added to dissolve the residues, and the solutions were allowed to evaporate slowly. Crystals suitable for single-crystal XRD were obtained over several weeks. The mixtures afforded a variety of crystals of varying compositions determined by single-crystal XRD analysis to be $[Pr(CyMe_4\text{-}BTBP)_2(NO_3)](NO_3)_2{\cdot}4EtOH{\cdot}H_2O$ (**6**·$4EtOH{\cdot}H_2O$), $[Pr(CyMe_4\text{-}BTBP)_2(NO_3)]_2[Pr(NO_3)_6](NO_3){\cdot}6CH_3CN$ (**7**·$6CH_3CN$), $[Eu(CyMe_4\text{-}BTBP)_2(NO_3)](NO_3)_2{\cdot}4EtOH{\cdot}2H_2O$ (**8**·$4EtOH{\cdot}2H_2O$), $[Eu(CyMe_4\text{-}BTBP)(NO_3)_3]$·toluene (**9**·toluene), and $[Tb(CyMe_4\text{-}BTBP)_2(H_2O)](NO_3)_2{\cdot}4EtOH$ (**10**·4EtOH). Bulk analysis of the crystallized samples by ESI-MS provided the following data:-

ESI-MS (positive ion): Pr^{3+} complexation, m/z 635 ($[[(C_{32}H_{38}N_8)_2(NO_3)Pr]^{2+}$); Eu^{3+} complexation, m/z 641 ($[[(C_{32}H_{38}N_8)_2(NO_3)Eu]^{2+}$); Tb^{3+} complexation, m/z 643 ($[[(C_{32}H_{38}N_8)_2(NO_3)Tb]^{2+}$).

Solution Preparation for UV−visible Spectroscopic Studies of Ln^{3+} Complexation with $CyMe_4$-BTPhen and $CyMe_4$-BTBP. Methanolic solutions of the ligands $CyMe_4$-BTBP and $CyMe_4$-BTPhen (1.0×10^{-4} M, 0.4 mL) were added to a quartz cuvette of 1 cm path length, and the solutions were diluted to 2 mL with MeOH (2.0×10^{-5} M). At this point, an initial spectrum of the ligand was recorded. Metal solutions of $Eu(NO_3)_3{\cdot}6H_2O$, $Pr(NO_3)_3{\cdot}6H_2O$, and $Tb(NO_3)_3{\cdot}5H_2O$ (4.0×10^{-4} M) in MeOH were used. For each titration, the metal solution was added into the cuvette in 10 μL (4.0×10^{-9} mol, 0.10 equiv) aliquots and shaken, and spectra were recorded after each addition up to a ratio of 1.5:1 metal/ligand. At this point, the aliquot size was increased to 50 μL (0.50 equiv) to a final ratio of 3:1 metal/ligand.

Solution Preparation for Luminescence Studies of Ln^{3+} (Ln = Pr, Tb, Eu) Complexation with $CyMe_4$-BTPhen and $CyMe_4$-BTBP. A solution of $CyMe_4$-BTPhen/$CyMe_4$-BTBP in MeOH (120 μL, 1×10^{-4} M) was added to a 1.2 mL quartz cuvette followed by the addition of a solution of $Ln(NO_3)_3$ in MeOH (20 μL, 3×10^{-4} M). The solution was diluted to ∼1 mL with MeOH, and spectra were obtained.

Solution samples in MeOH-d_4 were prepared in the same manner as that for the MeOH samples but using a 6×10^{-4} M solution of $CyMe_4$-BTPhen/$CyMe_4$-BTBP (20 μL) in MeOH-d_4, and solutions were diluted using MeOH-d_4.

Extracted Sample Preparation for XAS Measurements. Predistilled cyclohexanone and a 30% (v/v) solution of TBP in cyclohexanone were "washed" before use according to previously outlined procedures.[41] The washing of the organic solvent took place 4 days before lanthanide extractions were performed. The extractants $CyMe_4$-BTBP and $CyMe_4$-BTPhen were dissolved in either solvent system by gentle warming and sonication to a final extractant concentration of 50 mM. Aqueous stock solutions of $Ln(NO_3)_3$ (Ln = Pr, Eu, Tb; 10 mM) were prepared by dissolution of the relevant salt in 4 M HNO_3 in deionized H_2O for extractions with 30% TBP/cyclohexanone, while an aqueous mixture of 1 M HNO_3 and 3 M $NaNO_3$ in deionized water was used for extractions with pure cyclohexanone because of previously reported miscibility issues.[22]

The extractions were performed using 1.0 mL of each phase (organic and aqueous) contained in a 2.5 mL sample vial. The phases were mixed using a Labinco L46 shaker for 5 min each. Once contacted, each sample had the (lower) aqueous layer syringed out of the vial and then the (upper) organic layer pipetted into another vial for storage before XAS measurements were performed.

Solid Sample Preparation for XAS Measurements. Solid samples of **2**−**4** were prepared for XAS measurements by crushing ∼5−6 mg of the crystalline material in a mortar and pestle and mixed thoroughly with ∼90 mg of BN. The homogeneous material was then pressed into flat disks (∼2 cm diameter).

X-ray Crystallography. Diffraction data for **1**·$10H_2O$, **2**·$1.63EtOH{\cdot}0.75H_2O$, **3**·$9H_2O$, **4**·$9H_2O$, **5**·$9H_2O$, **6**·$4EtOH{\cdot}H_2O$, **7**·$6CH_3CN$, **8**·$4EtOH{\cdot}2H_2O$, **9**·toluene, and **10**·4EtOH were measured at 100 K with either a Bruker APEX SMART platform CCD area Mo Kα diffractometer (**2**, **3**, and **9**), an Oxford Diffraction XCalibur2

dx.doi.org/10.1021/ic301599y | Inorg. Chem. XXXX, XXX, XXX−XXX

Mo Kα diffractometer (**1** and **4**–**8**), or a Bruker APEX2 Cu Kα diffractometer (**10**). All were equipped with a low-temperature device, and collections were performed at 100 K. *CryAlisPro* was used to guide the Oxford diffractometer for collection of a full set of diffraction images and perform unit cell determination and data reduction. These data were corrected for Lorenz and polarization factors, and analytical, multiscan, and absorption corrections were applied. Bruker *SMART* (Mo Kα) or *APEX2* (Cu Kα) was used to guide the Bruker diffractometers and perform unit cell determinations.[42] Reduction of the Bruker collected data was performed using *SAINT PLUS* (Mo Kα) or *APEX2* (Cu Kα), and a multiscan absorption correction was performed using *SADABS*.[43,44] For all crystal data, the structures were solved by direct methods using *SIR92*.[45] Structure refinement was achieved via full-matrix least squares based on F^2 using *SHELXL97*.[46] All non-H atoms not exhibiting disorder were refined anisotropically, while H atoms were included in calculated positions. Molecular graphics were generated using *ORTEP*, and all displayed plots show probability ellipsoids of 50%.[47] In the case of structure **10**, modeling of residual solvent molecules was not possible. As such, the *SQUEEZE* procedure in *PLATON* was used to obtain solvent-free reflection data, and subsequent refinement was performed on these data. The *PART* command was used to model disorder over multiple sites, where appropriate, and is detailed in the relevant CIF (crystallographic information) files (see the Supporting Information).

General XAS Measurements. Ln (Eu and Tb) L_{III}-edge XAS spectra of extracted solutions and crystalline solids were recorded in transmission and fluorescence modes on Beamline B18 at the Diamond Light Source operating in a 10 min top-up mode for a ring current of 300 mA and an energy of 3 GeV. The radiation was monochromated with a Si(111) double crystal, and harmonic rejection was achieved through the use of two platinum-coated mirrors operating at an incidence angle of 8.3 mrad. The monochromator was calibrated using the K-edge of an iron foil, taking the first inflection point in the Fe-edge as 7112 eV. Spectra obtained in fluorescence mode utilized a nine-element germanium detector. The spectra were summed and background-subtracted using the software package *Athena*.[48] The spectra were simulated using the software package *Artemis*, which utilizes the Feff database in its simulations.[48,49]

CONCLUSIONS

The successful characterization of a series of directly synthesized Ln^{III} complexes of the tetra-N-donor extractants $CyMe_4$-BTPhen and $CyMe_4$-BTBP using XRD for solid-state studies and solution electronic spectroscopy has provided robust chemical models, which can be used to assist in the determination of lanthanide species formed under proposed conditions for the partitioning of SNF. Fits of the EXAFS region from XAS spectra showed that the dominant species extracted into the organic phase were complex, where two N_4-donor extractant ligands were coordinated to the Ln^{3+} center, as is mainly observed in the direct synthesis studies. XAS was unable to elucidate the bound ligand at the ninth coordination site in these Ln^{3+} complexes, but luminescence spectroscopy indicates that nitrate coordination is preferred over water binding in organic solvents. The presence of TBP in the organic phase, which may be used in a potential GANEX separation, clearly showed no influence with regards to lanthanide speciation. Further work will assess the source of the high separation factors that these N-donor ligands exhibit for minor actinide/lanthanide partitioning. Similar speciation studies for extracted Am^{3+} and Cm^{3+} in the bulk organic phase will be performed to determine if minor actinide complexes analogous to those observed in the lanthanide studies are formed or whether separation is achieved by the formation of minor actinide species that are substantially different [e.g., charge-neutral tris(nitrate) complex molecules] from those of the lanthanides. Such studies have been performed for BTP-derived extractants and indicate little difference between Eu^{3+} and Cm^{3+} speciation,[50] but this needs to be confirmed for the N_4-donor extractants particularly with respect to the role of nitrate ions as the lanthanide series is traversed in minor actinide/lanthanide coordination. Studies investigating metal speciation at the interfacial region in these liquid–liquid separations will also be conducted to assess the mechanism by which the minor actinides preferentially cross from the aqueous phase into the organic phase using these organic-soluble N-donor extractants and whether actinide/lanthanide speciation in the bulk organic phase is different from that at the liquid–liquid interface. Understanding the molecular-scale processes that underpin techniques for the partitioning of SNF will provide improved development of advanced separation methodologies like SANEX and GANEX.

ASSOCIATED CONTENT

Supporting Information

Plots of single-crystal XRD structures, crystallographic information files (CIF), UV–visible absorption, excitation and emission spectra, ORTEP plots, and XAS spectra with corresponding fits and parameters for the EXAFS data region. This material is available free of charge via the Internet at http://pubs.acs.org.

AUTHOR INFORMATION

Corresponding Author

*E-mail: clint.a.sharrad@manchester.ac.uk. Tel: +44 161 275 4657. Fax: +44 161 306 9321.

Notes

The authors declare no competing financial interest.

ACKNOWLEDGMENTS

This work is funded by the RCUK Energy Programme through its support of the MBASE consortium and the Nuclear Fission Safety Program of the European Union through ACSEPT Contract FP7-CP-2007-211 267. The studentship for D.M.W. was provided by the EPSRC-funded Nuclear FiRST Doctoral Training Centre. We thank Diamond Light Source for access to Beamline B18 (SP7226), which contributed to the results presented here. We acknowledge use of the EPSRC-funded Chemical Database Service at Daresbury. We also thank Dr. John Charnock for his assistance with EXAFS simulations. Use of the Chemical Analysis Facility at the University of Reading and access to the Mass Spectrometry Service and the Microanalysis Laboratory at the University of Manchester are also acknowledged.

REFERENCES

(1) Denniss, I. S.; Jeapes, A. P. In *The Nuclear Fuel Cycle*; Wilson, P. D., Ed.; Oxford University Press: Oxford, U.K., 1986; pp 116–132.

(2) (a) Nash, K. L.; Choppin, G. R. *Sep. Sci. Technol.* **1997**, *32*, 255–274. (b) Sood, D. D.; Patil, S. K. *J. Radioanal. Nucl. Chem.* **1996**, *203*, 547–573.

(3) (a) Lanham, W. B.; Runion, T. C.*PUREX process for plutonium and uranium recovery*; USAEC report ORNL-479; Oak Ridge National Laboratory: Oak Ridge, TN, 1949. (b) Warf, J. C. *J. Am. Chem. Soc.* **1949**, *71*, 3257–3258. (c) Batey, W. In *Science and Practice of Liquid–Liquid Extraction*; Thompson, J. D., Ed.; Clarendon Press: Oxford, U.K., 1992; Vol. *2*, p 139.

(4) Paiva, A. P.; Malik, P. *J. Radioanal. Nucl. Chem.* **2004**, *261*, 485–496.

(5) Cocalia, V. A.; Jensen, M. P.; Holbrey, J. D.; Spear, S. K.; Stepinski, D. C.; Rogers, R. D. *Dalton Trans.* **2005**, 1966−1971.
(6) Warin, D. *IOP Conf. Ser.: Mater. Sci. Eng.* **2010**, *9*, 012063.
(7) Panak, P. J.; Geist, A. *Chem. Rev.* **2013**, DOI: 10.1021/cr3003399
(8) Madic, C.; Hudson, M. J.; Liljenzin, J.-O.; Glatz, J.-P.; Nannicini, R.; Facchini, A.; Kolarik, Z.; Odoj, R. *Prog. Nucl. Energy* **2002**, *40*, 523−526.
(9) Madic, C.; Boullis, B.; Baron, P.; Testard, F.; Hudson, M. J.; Liljenzin, J.-O.; Christiansen, B.; Ferrando, M.; Facchini, A.; Geist, A.; Modolo, G.; Espartero, A. G.; De Mendoza, J. *J. Alloys Compd.* **2007**, *444*−*445*, 23−27.
(10) Hudson, M. J.; Harwood, L. M.; Laventine, D. M.; Lewis, F. W. *Inorg. Chem.* **2013**, DOI 10.1021/ic3008848.
(11) Grouiller, J.-P.; Pillon, S.; de Saint Jean, C.; Varaine, F.; Leyval, L.; Vambenepe, G.; Carlier, B. *J. Nucl. Mater.* **2003**, *320*, 163−169.
(12) Geist, A.; Hill, C.; Modolo, G.; Foreman, M. R. St. J.; Weigl, M.; Gompper, K.; Hudson, M. J. *Solvent Extr. Ion Exch.* **2006**, *24*, 463−483.
(13) Nilsson, M.; Nash, K. *Solvent Extr. Ion Exch.* **2007**, *25*, 665−701.
(14) Gelis, A. V.; Vandegrift, G. F.; Bakel, A.; Bowers, D. L.; Hebden, A. S.; Pereira, C.; Regalbuto, M. *Radiochim. Acta* **2009**, *97*, 231−232.
(15) (a) Mincher, B. J.; Schmitt, N. C.; Case, M. E. *Solvent Extr. Ion Exch.* **2011**, *29*, 247−259. (b) Vandegrift, G. F.; Chamberlain, D. B.; Connor, C.; Copple, J. M.; Dow, J. A.; Everson, L.; Hutter, J. C.; Leonard, R. A.; Nunez, L.; Regalbuto, M. C.; Sedlet, J.; Srinivasan, B.; Weber, S.; Wygmans, D. G. Proceedings of the Symposium on Waste Management, Tuscon, AZ, 1993.
(16) Brown, J.; Carrott, M. J.; Fox, O. D.; Maher, C. J.; Mason, C.; McLachlan, F.; Sarsfield, M. J.; Taylor, R. J.; Woodhead, D. A. *IOP Conf. Ser.: Mater. Sci. Eng.* **2010**, *9*, 012075.
(17) (a) Kolarik, Z.; Müllich, U.; Gassner, F. *Solvent Extr. Ion Exch.* **1999**, *17*, 23−32. (b) Kolarik, Z.; Müllich, U.; Gassner, F. *Solvent Extr. Ion Exch.* **1999**, *17*, 1155−1170. (c) Drew, M. G. B.; Guillaneux, D.; Hudson, M. J.; Iveson, P. B.; Russell, M. L.; Madic, C. *Inorg. Chem. Commun.* **2001**, *4*, 12−15.
(18) (a) Drew, M. G. B.; Foreman, M. R. S. J.; Hill, C.; Hudson, M. J.; Madic, C. *Inorg. Chem. Commun.* **2005**, *8*, 239−241. (b) Foreman, M. R. S. J.; Hudson, M. J.; Geist, A.; Madic, C.; Weigl, M. *Solvent Extr. Ion Exch.* **2005**, *23*, 645−662.
(19) (a) Magnusson, D.; Christiansen, B.; Foreman, M. R. S.; Geist, A.; Glatz, J.-P.; Malmbeck, R.; Modolo, G.; Serrano-Purroy, D.; Sorel, C. *Solvent Extr. Ion Exch.* **2009**, *27*, 97−106. (b) Magnusson, D.; Christiansen, B.; Malmbeck, R.; Glatz, J.-P. *Radiochim. Acta* **2009**, *97*, 497−502.
(20) Lewis, F. W.; Harwood, L. M.; Hudson, M. J.; Drew, M. G. B.; Desreux, J. F.; Vidick, G.; Bouslimani, N.; Modolo, G.; Wilden, A.; Sypula, M.; Vu, T.-H.; Simonin, J.-P. *J. Am. Chem. Soc.* **2011**, *133*, 13093−13102.
(21) Brown, J.; McLachlan, F.; Sarsfield, M.; Taylor, R.; Modolo, G.; Wilden, A. *Solvent Extr. Ion Exch.* **2012**, *30*, 127−141.
(22) Aneheimmgrt, E.; Ekberg, C.; Fermvik, A.; Foreman, M. R. St. J.; Retegan, T.; Skarnemark, G. *Solvent Extr. Ion Exch.* **2010**, *28*, 437−458.
(23) Foreman, M. R. S.; Hudson, M. J.; Drew, M. G. B.; Hill, C.; Madic, C. *Dalton Trans.* **2006**, 1645−1653.
(24) Steppert, M.; Cisařová, I.; Fanghänel, T.; Geist, A.; Lindqvist-Reis, P.; Panak, P.; Štěpnička, P.; Trumm, S.; Walther, C. *Inorg. Chem.* **2012**, *51*, 591−600.
(25) Retegan, T.; Berthon, L.; Ekberg, C.; Fermvik, A.; Skarnemark, G.; Zorz, N. *Solvent Extr. Ion Exch.* **2009**, *27*, 663−682.
(26) Lewis, F. W.; Harwood, L. M.; Hudson, M. J.; Drew, M. G. B.; Sypula, M.; Modolo, G.; Whittaker, D.; Sharrad, C. A.; Videva, V.; Hubscher-Bruder, V.; Arnaud-Neu, F. *Dalton Trans.* **2012**, *41*, 9209−9219.
(27) Hubscher-Bruder, V.; Haddaoui, J.; Bouhroum, S.; Arnaud-Neu, F. *Inorg. Chem.* **2010**, *49*, 1363−1371.
(28) (a) Vacca, A., Sabatini, A.; Gans, P. *Hyperquad2006*, version 3.1.48; Protonic Software Corp.: Dallas, TX, 2006. (b) Gans, P.; Sabatini, A.; Vacca, A. *Talanta* **1996**, *43*, 1739−1753.
(29) Natrajan, L. S.; Khoabane, N. M.; Dadds, B. L.; Muryn, C. A.; Pritchard, R. G.; Heath, S. L.; Kenwright, A. M.; Kuprov, I.; Faulkner, S. *Inorg. Chem.* **2010**, *49*, 7700−7709.
(30) Pathak, P. N.; Ansari, S. A.; Godbole, S. V.; Dhobale, A. R.; Manchanda, V. K. *Spectrochim. Acta A* **2009**, *73*, 348−352.
(31) (a) Richardson, F. S. *Chem. Rev.* **1982**, *82*, 541−552. (b) Natrajan, L. S.; Blake, A. J.; Wilson, C.; Weinstein, J. A.; Arnold, P. L. *Dalton Trans.* **2004**, 3748−3755.
(32) Trumm, S.; Lieser, G.; Foreman, M. R. S. J.; Panak, P. J.; Geist, A.; Fanghänel, T. *Dalton Trans.* **2010**, *39*, 923−929.
(33) Tedeshi, C.; Picaud, C.; Azéma, J.; Donnadieu, B.; Tisnès, P. *New J. Chem.* **2000**, *24*, 735−737.
(34) (a) Beeby, A.; Clarkson, I. M.; Dickins, R. S.; Faulkner, S.; Parker, D.; Royle, L.; de Sousa, A. S.; Williams, J. A. G.; Woods, M. *J. Chem. Soc., Perkin Trans. 2* **1999**, 493−503. (b) Zhao, Y.-F.; Zhao, Y.-L.; Bai, F.; Wei, X.-Y.; Zhou, Y.-S.; Shan, M.-N.; Li, H.-H.; Ma, R.-J.; Fu, X.-T.; Du, Y. *J. Fluoresc.* **2010**, *20*, 763−770.
(35) (a) Fletcher, D. A.; McMeeking, R. F.; Parkin, D. *J. Chem. Inf. Comput. Sci.* **1996**, *36*, 746−749. (b) Allen, F. H. *Acta Crystallogr.* **2002**, *B58*, 380−388. (c) Bruno, I. J.; Cole, J. C.; Edgington, P. R.; Kessler, M.; Macrae, C. F.; McCabe, P.; Pearson, J.; Taylor, R. *Acta Crystallogr.* **2002**, *B58*, 389−397. (d) Macrae, C. F.; Edgington, P. R.; McCabe, P.; Pidcock, E.; Shields, G. P.; Taylor, R.; Towler, M.; van de Streek, J. *J. Appl. Crystallogr.* **2006**, *39*, 453−457.
(36) (a) Cotton, S. A.; Franckevicius, V.; Mahon, M. F.; Ling Ooi, L.; Raithby, P. R.; Teat, S. J. *Polyhedron* **2006**, *25*, 1057−1068. (b) Kaczmarek, A. M.; Kubicki, M.; Pospieszna-Markiewicz, I.; Radecka-Paryzek, W. *Inorg. Chim. Acta* **2011**, *365*, 137−142. (c) Merkel, M.; Pascaly, M.; Köster, C.; Krebs, B. *Z. Naturforsch. B* **2004**, *59*, 216−220.
(37) (a) Berthet, J.-C.; Thuéry, P.; Foreman, M. R. S.; Ephritikhine, M. *Radiochim. Acta* **2008**, *96*, 189−197. (b) Berthet, J.-C.; Thuéry, P.; Dognon, J.-P.; Guillaneux, D.; Ephritikhine, M. *Inorg. Chem.* **2008**, *47*, 6850−6862. (c) Berthet, J.-C.; Maynadié, J.; Thuéry, P.; Ephritikhine, M. *Dalton Trans.* **2010**, *39*, 6801−6807.
(38) (a) Gregloński, G.; Lisowski, L. *Angew. Chem., Int. Ed.* **2006**, *45*, 6122−6126. (b) Visinescu, D.; Fabelo, O.; Ruiz-Pérez, C.; Lloret, F.; Julve, M. *CrystEngComm* **2010**, *12*, 2454−2465.
(39) (a) Feng, M.-L.; Mao, J.-G. *Eur. J. Inorg. Chem.* **2007**, *34*, 5447−5454. (b) Zhou, X.-H.; Peng, Y.-H.; Du, X.-D.; Wang, C.-F.; Zuo, J.-L; You, X.-Z. *Cryst. Growth Des.* **2009**, *9*, 1028−1035. (c) Zhang, Z.-J.; Shi, W.; Huang, Y.-Q.; Zhao, B.; Cheng, P.; Liao, D.-Z.; Yan, S.-P. *CrystEngComm* **2009**, *11*, 1811−1814.
(40) Lam, A. W.-H.; Wong, W.-T.; Wen, G.; Zhang, X.-X.; Gao, S. *New J. Chem.* **2001**, *25*, 531−533.
(41) Sarsfield, M. J.; Taylor, R. J.; Maher, C. J. *Radiochim. Acta* **2007**, *95*, 677−682.
(42) *SMART*, version 5.625; Bruker AXS Inc.: Madison, WI, 2001.
(43) *SAINT*, version 6.36a; Bruker AXS Inc.: Madison, WI, 2002.
(44) *SADABS*, version 2.03a; Bruker AXS Inc.: Madison, WI, 2001.
(45) Altomare, A.; Cascarano, G.; Giacovazzo, C.; Guagliardi, A. *J. Appl. Crystallogr.* **1993**, *26*, 343−350.
(46) Sheldrick, G. M. *SHELXL97, Programs for Crystal Structure Analysis*, release 97-2; University of Göttingen: Göttingen, Germany, **1998**.
(47) Farrugia, L. J. *J. Appl. Crystallogr.* **1997**, *30*, 565.
(48) Ravel, B.; Newville, M. *J. Synchrotron Radiat.* **2005**, *12*, 537−541.
(49) Newville, M. *J. Synchrotron Radiat.* **2001**, *8*, 322−324.
(50) Denecke, M. A.; Rossberg, A.; Panak, P. J.; Weigl, M.; Schimmelpfennig, B.; Geist, A. *Inorg. Chem.* **2005**, *44*, 8418−8425.